



## Diurnal changes in perineuronal nets and parvalbumin neurons in the rat medial prefrontal cortex

John H Harkness, Angela E Gonzalez, Priyanka N Bushana, Emily T Jorgensen, Deborah M Hegarty, Ariel A Di Nardo, Alain Prochiantz, Jonathan P Wisor, Sue A Aicher, Travis E Brown, et al.

### ► To cite this version:

John H Harkness, Angela E Gonzalez, Priyanka N Bushana, Emily T Jorgensen, Deborah M Hegarty, et al.. Diurnal changes in perineuronal nets and parvalbumin neurons in the rat medial prefrontal cortex. *Brain Structure and Function*, 2021, 226, pp.1135 - 1153. 10.1007/s00429-021-02229-4 . hal-03428849

**HAL Id: hal-03428849**

**<https://hal.science/hal-03428849>**

Submitted on 18 Nov 2021

**HAL** is a multi-disciplinary open access archive for the deposit and dissemination of scientific research documents, whether they are published or not. The documents may come from teaching and research institutions in France or abroad, or from public or private research centers.

L'archive ouverte pluridisciplinaire **HAL**, est destinée au dépôt et à la diffusion de documents scientifiques de niveau recherche, publiés ou non, émanant des établissements d'enseignement et de recherche français ou étrangers, des laboratoires publics ou privés.

# Diurnal changes in perineuronal nets and parvalbumin neurons in the rat medial prefrontal cortex

John H. Harkness<sup>\*1,2</sup> Angela E. Gonzalez<sup>\*1,2</sup>, Priyanka N. Bushana<sup>3</sup>, Emily T. Jorgensen<sup>4</sup>,  
Deborah M. Hegarty<sup>5</sup>, Ariel A. Di Nardo<sup>6</sup>, Alain Prochiantz<sup>6</sup>, Jonathan P. Wisor<sup>3</sup>,  
Sue A. Aicher<sup>5</sup>, Travis E. Brown<sup>4</sup>, and Barbara A. Sorg<sup>1,2</sup>

<sup>1</sup>Department of Integrative Physiology and Neuroscience, Washington State University  
Vancouver, Washington, 98686; <sup>2</sup>Dow Neurobiology, Legacy Research Institute, Portland,  
Oregon, 97239; <sup>3</sup>Department of Biomedical Sciences, Elson S. Floyd College of Medicine,  
Washington State University Spokane, Washington, 99202; <sup>4</sup>Department of Pharmaceutical  
Science, University of Wyoming, Laramie, WY, 82071, <sup>5</sup> Department of Chemical Physiology  
and Biochemistry, Oregon Health & Science University, Portland, Oregon, 97239; <sup>6</sup>Centre for  
Interdisciplinary Research in Biology, Collège de France, CNRS UMR 7241, INSERM U1050,  
PSL Research University, Labex MemoLife 75005 Paris, France

\*Denotes equal authorship

## *Corresponding Author:*

Barbara A. Sorg, Ph.D.  
Dow Neurobiology, Legacy Research Institute  
1225 NE 2<sup>nd</sup> Ave 34  
Portland, OR 97232  
PH: 503-413-1934  
FX: 503-413-5465  
bsorg@downeurobiology.org  
ORCID ID# 0000-0002-4913-4910

## ABSTRACT

Perineuronal nets (PNNs) surrounding fast-spiking, parvalbumin (PV) interneurons provide excitatory:inhibitory balance within cortical circuits. This balance is impaired in several disorders that are also associated with altered diurnal rhythms, yet few studies examined diurnal rhythms of PNNs or PV cells. We measured the intensity and number of PV cells and PNNs labeled with *Wisteria floribunda* agglutinin (WFA) and also the oxidative stress marker 8-oxo-deoxyguanosine (8-oxo-dG) in rat prelimbic medial prefrontal cortex (mPFC) at Zeitgeber times (ZT) ZT0, 6, 12, and 18. Relative to ZT0, the intensities of PNN and PV labeling were increased in the dark (active) phase compared with the light (inactive) phase. The intensity of 8-oxo-dG was decreased from ZT0 at all times (ZT6,12,18). To examine changes in inhibitory and excitatory inputs to PV cells, we measured GAD 65/67 and vGLUT1 puncta apposed to PV cells with and without PNNs. There were more excitatory puncta on PV cells with PNNs at ZT18 vs. ZT6, but no changes in PV cells without PNNs and no changes in inhibitory puncta. Whole-cell slice recordings in fast-spiking (PV) cells with PNNs showed an increased ratio of  $\alpha$ -amino-3-hydroxy-5-methyl-4-isoxazolepropionic acid receptor:N-methyl-D-aspartate receptor (AMPA:NMDA) at ZT18 vs. ZT6. The number of PV cells and PV/PNN cells containing orthodenticle homeobox 2 (OTX2), which maintains PNNs, showed a strong trend toward an increase from ZT6 to ZT18. Diurnal fluctuations in PNNs and PV cells are expected to alter cortical excitatory:inhibitory balance and provide new insights into treatments for diseases impacted by disturbances in sleep and circadian rhythms.

## Keywords

Circadian; Diurnal; Medial prefrontal cortex; OTX2; Parvalbumin; Perineuronal nets

## **DECLARATIONS**

### **Funding:**

This work was funded by Washington State University Alcohol and Drug Abuse Research Program, NIH GM134789 (JHH); NIH DA033404 (BAS), DA040965 (BAS, TEB, SAA); NIH NS078498 (JPW); NIH P30 NS061800 (SAA); and Agence Nationale de la Recherche ANR-18-CE16-0013-01 (AP and AAD).

**Conflicts of interest:** JHH and BAS are listed as inventors of the Washington State University analysis program, Pipsqueak™. JHH is a majority stake holder in Rewire Neuro, Inc., the licensing partner of the *Pipsqueak*™ technology. The authors do not perceive these relationships to have had an influence on this report.

**Ethics approval:** All procedures were performed in accordance with the National Institutes of Health's Guidelines for the Care and Use of Laboratory Animals and with approval from the Institutional Animal Care and Use Committee at Legacy Research Institute and Washington State University.

**Consent to participate:** N/A

**Consent for publication:** N/A

**Availability of data and material:** Data are available upon request from the corresponding author.

**Code availability:** Available for download at <https://pipsqueak.ai>

**Authors' contributions:** JHH and AEE, ETJ, and DH conducted experiments and analyzed data; PNB analyzed data; JPW performed statistical analyses and contributed to writing the

manuscript; AD and AP contributed to writing the manuscript; and SAA, TEB, and BAS contributed to writing the manuscript, and designed and directed the experiments.

## INTRODUCTION

Perineuronal nets (PNNs) are specialized extracellular matrix structures that surround specific neurons in the brain and spinal cord (Hartig et al. 1992), appear during critical periods of development (Carulli et al. 2010; Balmer et al. 2009; Dityatev et al. 2007; Bruckner et al. 1993), and restrict plasticity during adulthood (Pizzorusso et al. 2002). PNNs surround mainly parvalbumin (PV)-containing, fast-spiking GABAergic interneurons in several brain regions (Seeger et al. 1994), including in the medial prefrontal cortex (mPFC) (Slaker et al. 2015). The prelimbic region of the mPFC is associated with working memory and cognition (Kolb et al. 1974; Braver et al. 1997). PV neurons profoundly inhibit the network of surrounding neurons via their elaborate contacts with local pyramidal neurons (Packer and Yuste 2011), thereby regulating plasticity associated with learning, decision making, attention, cognitive flexibility, and working memory (Ferguson and Gao 2018a; Cho et al. 2015; Ferguson and Gao 2018b; Murray et al. 2015). PV cells therefore contribute to essential excitatory:inhibitory balance for normal functioning of the mPFC (Ferguson and Gao 2018a) and are critical for generating gamma oscillations (Buzsaki and Draguhn 2004; Sohal et al. 2009; Cardin et al. 2009) believed to mediate normal working memory function and cognitive flexibility (Cho et al. 2015; Howard et al. 2003).

Perineuronal nets and PV neurons are important for normal learning and memory processes, and their dysfunction appears to contribute to a wide range of brain diseases/disorders, including schizophrenia, bipolar disorder, Alzheimer's disease, autism spectrum disorder, epilepsy, and disorders associated with drugs of abuse and fear (Sorg et al. 2016; Fawcett et al. 2019; Testa et al. 2019; Steullet et al. 2017; Lewis 2014; Pantazopoulos and Berretta 2016; Miyata and Kitagawa 2016; Rankin-Gee et al. 2015; Foscari et al. 2017; Gogolla et al. 2009; Goldman-Rakic 1994). Several of these disorders and cognitive impairments are also associated with circadian and/or sleep disturbances: most notably schizophrenia (Pantazopoulos et al. 2017; Seney et al. 2019; Wulff and Joyce 2011), autism spectrum disorder (Carmassi et al.

2019), epilepsy (Khan et al. 2018), drug use disorders (Chakravorty et al. 2018; Perreau-Lenz and Spanagel 2015; Logan et al. 2014), and neurodegenerative diseases such as Alzheimer's disease (Hood and Amir 2017; Fanjul-Moles and Lopez-Riquelme 2016). These disorders are all accompanied by poor working memory function and cognitive flexibility (Green et al. 2019; Elvevag and Goldberg 2000; Holmes 2015; Goldstein et al. 2009), functions that depend on optimal excitatory:inhibitory balance in the mPFC. The dynamics of cortical excitability are dependent on sleep homeostatic drive, which increases as the duration of prior wakefulness increases (Huber et al. 2013). More recently, these sleep-related effects are responsive to key dynamics in circadian rhythms, including the amplitude of these rhythms (Ly et al. 2016; Chellappa et al. 2016). Thus, a fundamental understanding of how PNNs and their underlying PV interneurons contribute to plasticity in response to outside stimuli, including diurnal physiological changes, is expected to provide new avenues for understanding and regulating excitatory:inhibitory balance in the mPFC.

We previously showed that sleep disruption in rats increased the intensity of the PNN marker, *Wisteria floribunda* agglutinin (WFA), PV, and the oxidative stress marker 8-oxo-2'-deoxyguanosine (8-oxo-dG) (Harkness et al. 2019). However, the magnitude of WFA changes were small, and we examined only one time of day when comparing sleep-disrupted rats with undisturbed controls. It is possible that these changes in marker intensity were masked by time-of-day changes created by diurnal fluctuations. Pantazopolous *et al.* (Pantazopoulos et al. 2020) recently reported that the number of PNNs in mice fluctuated diurnally in several brain regions, including the prelimbic mPFC, and that this same pattern persisted when mice were maintained under constant darkness, indicating a circadian influence. Here we tested the hypotheses that both PNN and PV intensity fluctuate diurnally. These fluctuations may reflect increased activity levels of rats during their active periods while facilitating greater synaptic plasticity during sleep. PNN and PV intensity were quantified in the prelimbic mPFC at four times of day (ZT0, ZT6,

ZT12, ZT18). In addition, we measured the intensity of 8-oxo-dG as an indicator of oxidative stress. We also hypothesized that glutamatergic signaling in WFA+/PV+ neurons would cycle between the light (ZT6) vs. the dark cycle (ZT18) and therefore we measured GAD65, GAD67, vGLUT1, and the volume of these neurons in the prelimbic mPFC at the same time points. Additionally, we measured the AMPA:NMDA ratio in fast-spiking/WFA+ neurons at ZT6 and ZT18 to determine if changes in excitatory inputs were reflected in changes in neuronal activity. Finally, at ZT6 and ZT18, we also assessed the number of cells containing orthodenticle homeobox 2 (OTX2), a homeoprotein transcription factor required for normal development of the CNS (Sakai et al. 2017; Di Nardo et al. 2018) that is imported by PNN-enwrapped PV cells (Beurdeley et al. 2012; Miyata et al. 2012; Bernard and Prochiantz 2016; Sugiyama et al. 2008). Our findings collectively indicate that several parameters of PV cells fluctuate diurnally, and these fluctuations have implications for altered excitatory:inhibitory balance in brain disorders with disrupted circadian rhythms and sleep.

## **METHODS**

### *Animals*

A total of 48 rats were used for the experiments. Male Sprague Dawley rats weighing 260-280 g were obtained from Envigo (Livermore, CA) and individually housed under LD12:12 conditions. Rats were maintained between 18° and 22°C and a relative humidity of 55%. Rats were allowed to acclimate to the light cycle for two weeks prior to euthanizing at four different times of day (see below). Protocols were approved by the Washington State University Institutional Animal Care and Use Committee (Protocol #07432). All efforts were made to reduce animal suffering.

### *Experimental design*

Rats were euthanized every 6 hours over four different time points, including Zeitgeber time (ZT)0, at lights-on, and ZT6, ZT12, and ZT18 (N = ZT0 (10), ZT6 (8), ZT12 (7), ZT18 (8)). Rats



were removed from the colony one at a time and within 30 sec to 1 min after removal, they were given an overdose of pentobarbital (50 mg/kg under brief, 5% isoflurane exposure) at the designated time point.

### *Immunohistochemistry*

Upon reaching unresponsiveness from pentobarbital overdose, rats were perfused transcardially with 150 mL 0.1M phosphate-buffered saline (PBS) at a rate of 300 mL/min. Perfusate was switched to 4% paraformaldehyde and rats were perfused at the same rate for 250 mL/rat. Brains were removed, immersed in 20 mL 4% paraformaldehyde overnight, and then immersed in 20% sucrose in PBS solution and refrigerated. After two days in sucrose solution (when the brains sank), brains were flash-frozen with powdered dry ice and stored at -80°C until sectioned.

Coronal sections containing the prelimbic PFC from +3.2 to +4.2 mm from bregma (Paxinos G 1998) were collected on a freezing microtome at 30 µm for a 1:8 section series (Slaker et al. 2016a). Triple-staining was performed by first washing a single series of free-floating sections three times for 5 min in PBS. Tissue was then treated with 50% ethanol for 30 min. Sections were washed in PBS three times for 5 min each before being placed in a blocking solution containing 3% normal goat serum (Vector Laboratories) for 1 hr. Subsequently, tissue was co-incubated with rabbit-anti-PV (ThermoFisher Scientific, Cat# PA1-933, RRID: AB\_2173898, 1:1000) and mouse-anti-8-oxo-dG (EMD Millipore, Cat# 4354-MC-050, RRID: AB\_2876794, 1:350) and 2% normal goat serum at 4°C overnight. Tissue was then rinsed in PBS three times for 10 min each and incubated for 2 hr in secondary antibodies (goat anti-rabbit Alexa Fluor® 405 for the PV antibody, (abcam, Cat# ab175652, RRID AB\_2687498, 1:500), goat anti-mouse Alexa Fluor® 594 for the 8-oxo-dG antibody (abcam, Cat# ab150120, RRID AB\_2650601, 1:500), and 2% normal goat serum. Slices were washed in PBS three times for 10

min each and then incubated with the fluorescein isothiocyanate (FITC)-conjugated PNN marker, *Wisteria floribunda* agglutinin (WFA, Vector Laboratories; Cat# FL-1351, AB\_2336875, 1:500), which is widely used to label PNNs (Hartig et al. 1992), and 2% normal goat serum at 4°C overnight. After three 10 min washes in PBS, sections were mounted onto Superfrost Plus slides and allowed to dry overnight. After drying, ProLong Gold Antifade Mountant (ThermoFisher Scientific) was applied to the slides before coverslipping.

We also measured OTX2 staining in a subset of brain slices used to measure WFA and PV. Owing to constraints in the protocol, we did not make comparisons of cell intensity and instead analyzed only cell numbers. After mounting to Superfrost Plus slides and brief drying, tissue sections were pretreated with 0.5% Triton-X and PBS solution followed by 100 mM glycine. Slides were washed three times with PBS, then bathed in blocking solution containing 5% BSA (Sigma) and 0.5% Triton-X in PBS for 30 minutes. Tissue was co-incubated with rabbit-anti-PV (as above) and mouse-anti-OTX-2 (1:25, in-house, Prochiantz Laboratory) in 5% BSA, 0.5% Triton-X in PBS in a humidified chamber at 4°C overnight. Tissue was then rinsed in PBS for 5 seconds and washed three times in PBS for 10 min each. Slices were incubated for 2 hr in a secondary antibody cocktail (goat anti-rabbit Alexa Fluor® 405 for the PV antibody and goat anti-mouse Alexa Fluor® 594 for the OTX-2 antibody, 1:500) in 5% BSA, 0.5% Triton-X in PBS. Tissue was then washed in PBS for 5 seconds, and three times for 10 min each. Finally, tissue was incubated in FITC-WFA (as above) in 5% BSA, 0.5% Triton-X in PBS for 2 hr at room temperature, washed in PBS for 5 seconds, and then washed three times for 10 min each. After drying, ProLong Gold Antifade Mountant (ThermoFisher Scientific) was applied to the slides before coverslipping.

### *Quantification of immunohistochemical images*

Imaging for WFA, PV, 8-oxo-dG, and OTX2 was performed on a Leica SP8 laser scanning confocal microscope with an HCX PL apo CS, dry, 20x objective with 0.70 numerical aperture. 405, 488, and 594 nm lasers were used for excitation, and were detected by three photomultiplier tubes in the 400-450, 460-510, and 590-640 nm ranges, respectively. Calibration of the laser intensity, gain, offset, and pinhole settings were determined within the orbitofrontal cortex of a control animal, as this region most reliably expresses strong WFA staining. These settings were maintained for all images. Images were collected in z-stacks of 20 images each (step size 0.44  $\mu\text{m}$ ; containing the middle 8.45  $\mu\text{m}$  of each brain section), encompassing the prelimbic PFC.

All images (1.194 pixels/ $\mu\text{m}$ ; 428 x 428  $\mu\text{m}$ ) were compiled into summed images using ImageJ macro plug-in Pipsqueak AI™ (<https://pipsqueak.ai>) (Slaker 2016), scaled, and converted into 8-bit, grayscale, tiff files. Pipsqueak AI™ was run in “semi-automatic mode” to select ROIs to identify individual PV+ cells, PNNs, 8-oxo-dG, or OTX2-labeled cells, which were then verified by a trained experimenter who was blinded to the experimental conditions. The plug-in compiles this analysis to identify single-(Slaker et al. 2016b), double-labeled (Jorgensen et al. 2020), and triple-labeled (Harkness et al. 2019) neurons. Labeling was quantified bilaterally in the prelimbic mPFC using Pipsqueak AI software. Background threshold levels were set and applied to all images for comparison. When describing co-labeling of PNNs with another cell marker (e.g., PV, OTX2 double- or triple-labeling), we acknowledge that WFA labeling is not strictly co-labeled but instead located around the perimeter of the markers located inside the cell.

### *Quantification of PV puncta and cell volume*

Because we generally found the maximal differences in PV and WFA labeling intensity between ZT6 (nadir) and ZT18 (peak), we assessed the number of excitatory and inhibitory puncta on PV

cells surrounded by PNNs at these two times of day. Immunohistochemistry and imaging were performed on brain slices from a subset of the animals used for WFA and PV intensity studies. Immunohistochemical methods were similar to those previously described (Slaker et al. 2018; Hegarty et al. 2014; Hegarty et al. 2010; Jorgensen et al. 2020). Solutions were prepared in either 0.1 M phosphate buffer at pH 7.4 (PB) or 0.1 M Tris-buffered saline at pH 7.6 (TS). Tissue sections were first rinsed in PB, then incubated in 1% sodium borohydride in PB for 30 min to reduce background. After rinses in PB and TS, sections were incubated in 0.5% bovine serum albumin (BSA) in TS for 30 min and then placed in a primary antibody cocktail made in 0.1% BSA and 0.25% Triton X-100 in TS for two nights at 4°C. The primary antibody cocktail consisted of mouse anti-glutamic acid decarboxylase 65 (GAD65, abcam, Cat# ab26113, RRID: AB\_448989, 1:500), mouse anti-glutamic acid decarboxylase 67 (GAD67, Millipore Sigma, Cat# MAB5406, RRID: AB\_2278725, 1:1000), rabbit anti-PV (Novus Biologicals, Cat# NB120-11427, RRID:AB\_791498, 1:1000), and guinea pig anti-vesicular glutamate transporter 1 (vGLUT1; EMD Millipore, Cat# AB5905, RRID: AB\_2301751, 1:5000). After 40 h primary antibody incubation, tissue sections were rinsed in TS and then incubated with a cocktail of fluorescently-labeled secondary antibodies for 2 h, light-protected, at room temperature. The secondary antibody cocktail consisted of Alexa Fluor 488 donkey anti-mouse (ThermoFisher Scientific, Cat# A21202, RRID: AB\_141607, 1:800) to label both GAD antibodies, Alexa Fluor 546 donkey anti-rabbit (ThermoFisher Scientific, Cat# A10040, RRID: AB\_2534016, 1:800); and Alexa Fluor 647 donkey anti-guinea pig (Jackson ImmunoResearch Laboratories, Cat# 706-605-148, RRID: AB\_2340476, 1:800). Tissue sections were rinsed again in TS and then incubated in biotinylated WFA (Vector Laboratories, Cat# B-1355, RRID: AB\_2336874, 1:50) for 2 h at room temperature. Following TS rinses, tissue sections were incubated for 3 h at room temperature in Alexa Fluor 405-conjugated streptavidin (ThermoFisher Scientific, Cat# S32351, 6.25 µg/ml). Finally, tissue sections were rinsed in TS followed by PB before being mounted with 0.05 M PB onto gelatin-coated slides to dry. Slides were coverslipped with Prolong Gold Antifade Mountant

(ThermoFisher Scientific) and light-protected until imaging. Anatomical landmarks were used to determine representative caudal and rostral sections of prelimbic cortex that were within bregma +3.5 to +4.2 mm (Paxinos G 1998).

Confocal imaging was performed as described previously (Slaker et al. 2018; Jorgensen et al. 2020). Two high magnification images were taken at each rostral-caudal level of the prelimbic mPFC (2 images/level x 2 levels/animal = 4 images/animal). Images were captured on a Zeiss LSM 780 confocal microscope with a 63 x 1.4 NA Plan-Apochromat objective (Carl Zeiss MicroImaging, Thornwood, NY) using the single pass, multi-tracking format at a 1024 x 1024 pixel resolution. Optical sectioning produced Z-stacks bounded by the extent of fluorescent immunolabeling throughout the thickness of each section. Using Zen software (Carl Zeiss, RRID SCR\_013672), PV neurons in each confocal stack were identified and assessed for the presence of a nucleus and whether the entire neuron was within the boundaries of the field of view; only these PV neurons were included in the analysis. The optical slice through the nucleus at which the ellipsoidal minor axis length of each PV neuron reached its maximum was determined. A Z-stack of that optical slice plus one optical slice above and one below was created resulting in a 1.15  $\mu\text{m}$  Z-stack through the middle of each PV neuron; these subset Z-stacks were used for puncta apposition analysis.

Image analysis of GABAergic and glutamatergic appositions onto PV-labeled neurons was performed as described (Slaker et al. 2018) using Imaris 9.0 software (BitPlane USA, Concord, MA, RRID: SCR\_007370) on an offline workstation in the Advanced Light Microscopy Core at Oregon Health & Science University by an observer who did not know experimental conditions. For each PV neuron, the manual setting of the *Surfaces* segmentation tool was used to trace the outline of the PV neuron in all three optical slices and a surface was created. The volume of the PV cell rendered model was measured by Imaris. To limit our analyses to the area

immediately surrounding each PV neuron, we used the *Distance Transform* function followed by the automated *Surfaces* segmentation tool to create another surface 1.5  $\mu\text{m}$  away from the PV neuron surface that followed the unique contours of that PV neuron. The *Mask Channel* function was then used to only examine WFA, GAD65/67 and vGLUT1 within this 1.5  $\mu\text{m}$ -wide perimeter surrounding the PV neuron surface.

The presence of WFA labeling in close proximity to the PV neuron surface was assessed for each PV neuron. A PV neuron was considered to have a PNN if there was any WFA labeling around any part of the PV neuron surface as seen by the observer. GAD65/67 and vGLUT1-labeled puncta were then assessed separately using the *Spots* segmentation tool. Within the *Spots* tool, the *Different Spot Sizes (Region Growing)* option was selected and initial settings included an estimated X-Y diameter of 0.5  $\mu\text{m}$  and an estimated Z plane diameter of 0.4  $\mu\text{m}$ . Spots generated by Imaris from these initial settings were then thresholded using the *Classify Spots, Quality Filter* histogram to ensure that all labeled puncta were included and background labeling was filtered out. The spots were then thresholded using the *Spot Region, Region Threshold* histogram to ensure that the sizes of the Imaris-generated spots were good approximations of the size of the labeled puncta seen visually by the human observer. Using the *Find Spots Close to Surface Imaris XTension*, we then isolated those spots that were within 0.5  $\mu\text{m}$  of the PV neuron surface. All segmented spots close to the PV neuron surface had to have a Z diameter of at least 0.4  $\mu\text{m}$  to be considered puncta (Hegarty et al. 2014; Hegarty et al. 2010).

### *Synaptic Electrophysiology*

To determine whether there was a change in glutamatergic transmission associated with the nadir (ZT6) and peak (ZT18) periods of PV and PNN staining intensity, a separate cohort of 15 rats was used to measure whole-cell electrophysiology on coronal slices (300  $\mu\text{m}$  collected at

3.2-3.7 mm from bregma) through the prelimbic mPFC. Only one cell per rat was used for each experiment so that reported N-sizes represent the number of animals. Recording conditions and solutions for whole-cell recordings were as previously described (Slaker et al. 2018; Jorgensen et al. 2020). Rats were briefly anesthetized with isoflurane and intracardially perfused with ice cold recovery solution: (in mM) 93 NMDG, 2.5 KCl, 1.2 NaH<sub>2</sub>PO<sub>4</sub>, 30 NaHCO<sub>3</sub>, 20 HEPES, 25 glucose, 4 sodium ascorbate, 2 thiourea, 3 sodium pyruvate, 10 MgSO<sub>4</sub>(H<sub>2</sub>O)<sub>7</sub>, 0.5 CaCl<sub>2</sub>(H<sub>2</sub>O)<sub>2</sub>, and HCl added until pH was 7.3-7.4 with an osmolarity of 300-310 mOsm. Slices were prepared on a vibratome (Leica VT1200S) containing recovering solution and then transferred to a holding chamber containing holding solution: (in mM) 92 NaCl, 2.5 KCl, 1.2 NaH<sub>2</sub>PO<sub>4</sub>, 30 NaHCO<sub>3</sub>, 20 HEPES, 25 glucose, 4 sodium ascorbate, 2 thiourea, 3 sodium pyruvate, 2 MgSO<sub>4</sub>(H<sub>2</sub>O)<sub>7</sub>, 2 CaCl<sub>2</sub>(H<sub>2</sub>O)<sub>2</sub>, and 2 M NaOH added until pH reached 7.3-7.4 and osmolarity was 300-310 mOsm. Slices remained in the holding chamber for at least 1 h prior to recording. PNN-surrounded fast-spiking interneurons were identified by incubating each slice in holding solution containing FITC-WFA (1 µg/mL) 5 min prior to recording and using CellSens software (Olympus) to identify cells surrounded by fluorescence. The fast-spiking interneurons in this region of the cortex are highly likely to be PV-containing cells (Kawaguchi and Kubota 1993). The recording chamber was continuously perfused at 31.0°C at a rate of 4-7 mL/min with artificial cerebrospinal fluid (aCSF): (in mM) 119 NaCl, 2.5 KCl, 1 NaH<sub>2</sub>PO<sub>4</sub>, 26 NaHCO<sub>3</sub>, 11 dextrose, 1.3 MgSO<sub>4</sub>(H<sub>2</sub>O)<sub>7</sub>, and 2.5 CaCl<sub>2</sub>(H<sub>2</sub>O)<sub>2</sub>. Patching pipettes were pulled from borosilicate capillary tubing (Sutter Instruments, CA USA) and the electrode resistance was typically 4-7 mOhms. All experiments utilized cesium chloride (CsCl) internal solution: (in mM) 117 CsCl, 2.8 NaCl, 5 MgCl<sub>2</sub>, 20 HEPES, 2 Mg<sup>2+</sup>ATP, 0.3 Na<sup>2+</sup>GTP, 0.6 EGTA, 0.1 spermine and sucrose to bring osmolarity to 275-280 mOsm and pH to ~7.25. For AMPA:NMDA ratios, neurons were held at +45 mV in 100 µM picrotoxin and 50 µM D-(-)-2-amino-5-phosphonopentanoic acid (d-APV) was added once a stable baseline was acquired. Peak AMPAR excitatory postsynaptic current (EPSC) amplitudes were measured at 20-25 min in d-

APV, and this EPSC was subtracted from 5 min averages of baseline EPSCs to obtain the peak NMDAR EPSC (Dingess et al. 2017). NMDA kinetics were calculated by measuring the time from peak to half peak (Brown et al. 2011). All drugs and reagents were obtained from Sigma-Aldrich (St Louis, MO).

### *Statistical analysis*

For PV, WFA, and 8-oxo-dG staining intensities, distributions of normalized intensities were compared within cell marker between experimental groups using the Kruskal-Wallis test to assess changes among the four ZT times, with all values normalized to ZT0. A Dunn's multiple comparisons test was used in the case of a significant effect. For comparison among ZTs and each cellular marker (Figure 2), a two-way ANOVA was done and was followed by a post-hoc Bonferroni test in the case of a significant interaction. A Komogorov-Smirnov test was used for comparison of distribution of labeling intensity between two groups. To determine the number of cells expressing each combination of markers, including OTX2, the number of cells was averaged per rat and the results were subjected to a one-way ANOVA followed by a Dunnett's multiple comparisons test in the case of 4 groups. In cases where comparisons were made between two groups, an unpaired t-test was performed. For puncta analysis, an unpaired t-test was performed or in the case of non-normal distribution, a Mann-Whitney test was performed. TIBCO Software Statistica 13.2 (2016) and GraphPad Prism 8 were used for all intensity, cell number, and puncta analyses. For electrophysiology experiments, unpaired t-tests were used to analyze AMPA:NMDA ratio and NMDA decay rates using Prism 6 (GraphPad Software). Differences were considered significant if  $p < 0.05$ .



## RESULTS

### *Diurnal fluctuation of PV and PNN intensity*

Both PV and WFA intensity fluctuated in a diurnal manner (Fig. 1). Fig. 1a shows an image of single- and double-labeled WFA and PV cells. Fig. 1b and c show cell intensity measures for total WFA+ cells (single-labeled WFA+ cells, including both PV+ and non-PV cells surrounded by WFA) and the double-labeled WFA+/PV+ subset of WFA+ cells. We first tested whether there was a difference between intensities in the light phase (ZT0, ZT6) vs. the dark phase (ZT12, ZT18). For WFA+ intensity, there was an effect of the light phase (ZT0, ZT6) vs. dark phase (ZT12, ZT18), with increased intensity in the dark phase ( $p < 0.0001$ ). Fig. 1b shows an effect of ZT ( $p < 0.0001$ ), with staining intensity of total WFA+ cells increased relative to ZT0: there was a 27% increase at ZT12 ( $p < 0.0001$ ) and a 40% increase at ZT18 ( $p < 0.0001$ ). Fig. 1c demonstrates a similar pattern for WFA+/PV+ cells, where there was an effect of the light phase (ZT0, ZT6) vs. dark phase (ZT12, ZT18), with increased labeling intensity in the dark phase ( $p < 0.0001$ ). Fig. 1c also shows that the increases in WFA intensity across the diurnal cycle in WFA+/PV+ double-labeled cells demonstrated an effect of ZT ( $p < 0.0001$ ) that was similar to that of total WFA+ cells (Fig. 1b), with a 23% increase at ZT12 ( $p < 0.0001$ ) and a 44% increase at ZT18 ( $p < 0.0001$ ).

Fig. 1d and 1e show the patterns of PV labeling intensity in total PV+ cells and those PV+ cells surrounded by WFA (PV+/WFA+). Similar to the WFA studies, we tested whether there was a light vs. dark phase difference in PV labeling intensity. Total PV+ cells showed a non-significant but strong trend of the light phase (ZT0, ZT6) vs. dark phase (ZT12, ZT18) ( $p < 0.0624$ ). The labeling intensity of PV+/WFA+ cells showed lower intensity during the light vs. dark phase ( $p < 0.0001$ ). There was an effect of ZT on PV+/WFA+ labeling intensity ( $p < 0.0001$ ), with a 24% decrease in intensity at ZT6 relative to ZT0 ( $p < 0.0001$ ).

The number of total WFA+ cells, total PV+ cells, and subsets of cells that were labeled with one or both markers, as well as the percent of co-labeled cells, are presented in Table 1. There was no difference in the number of total WFA+ cells or WFA+/PV- cells across ZT when either comparing the light phase (ZT0, ZT6) with the dark phase (ZT12, ZT18) or when comparing across the four ZTs. The number of total PV+ cells and WFA+/PV+ cells tended toward a change across ZTs ( $p = 0.0772$ ;  $p = 0.0517$ , respectively). We also examined the percent of WFA+ cells containing PV and *vice versa* and found no overall light vs. dark phase effects. For the percent of WFA+ cells that contained PV, there was an effect of ZT ( $p = 0.022$ ), with a range from 35-58% across ZTs, and a significant decrease at ZT6 relative to ZT0 ( $p = 0.011$ ). The percent of PV+ cells surrounded by WFA was consistent across ZTs, ranging from 45-47%. Overall, evaluation of PNNs and PV cells indicate that the intensities of both PNNs and PV cells increased in the dark phase.

#### *Diurnal fluctuation of 8-oxo-dG intensity*

We assessed the number of 8-oxo-dG+ cells in a subset of rats shown in Fig. 1. Fig. 2a shows a region of mPFC containing 8-oxo-dG+, WFA+, and PV+ single, double, and triple-labeled cells. The intensity of total 8-oxo-dG+ cells is shown in Fig. 2b, and we tested whether there was a light vs. dark phase difference. There was an effect of the light phase (ZT0, ZT6) vs. dark phase (ZT12, ZT18), with decreased intensity in the dark phase ( $p < 0.0001$ ). There was an effect of ZT on 8-oxo-dG intensity ( $p < 0.0001$ ), with a decrease at all ZTs relative to ZT0 ( $p < 0.0001$  for all ZTs), with a maximal 47% decrease at ZT12 vs. ZT0. The significant decrease in intensity of 8-oxo-dG was maintained at ZT18, with a 27% decrease vs. ZT0. Fig. 2c shows the intensity of 8-oxo-dG in 8-oxo-dG+/WFA+/PV+ triple-labeled cells, with an effect of light vs. dark phase ( $p < 0.0001$ ) and an effect of ZT ( $p < 0.0001$ ). These triple-labeled cells showed a 20-25% decrease in intensity of 8-oxo-dG at all three ZTs relative to ZT0 ( $p < 0.0001$  for all ZTs). Comparison of total 8-oxo-dG+ cells with 8-oxo-dG+/WFA+/PV+ triple-labeled cells showed a main effect of cellular subtype (single- vs. triple-label)

across ZTs ( $F_{1,22,121} = 133.5$ ,  $p < 0.0001$ ), a main effect of ZT ( $F_{2,22,121} = 38.6$ ,  $p < 0.0001$ ), and a cell subtype x ZT interaction ( $F_{2,22,121} = 10.23$ ,  $P < 0.0001$ ), with an increase in 8-oxo-dG intensity in triple vs. total 8-oxo-dG+ cells at all ZTs ( $p < 0.0001$  for both; not shown).

This increase in intensity of 8-oxo-dG in triple-labeled cells may be due to either the presence of PNNs, the presence of PV, or both, so we separately analyzed the intensity of 8-oxo-dG in 8-oxo-dG+/WFA+ cells and 8-oxo-dG+/PV+ cells across ZTs. The intensity of 8-oxo-dG in 8-oxo-dG+/WFA+ cells shown in Fig. 2d indicates an effect of light vs. dark phase ( $p < 0.0001$ ) as well as an effect of ZT ( $p < 0.0001$ ). As with single- and triple-labeled cells, the intensity of 8-oxo-dG in cells with WFA+ was reduced at all ZTs relative to ZT0 ( $p < 0.0001$  for all ZTs). The intensity of 8-oxo-dG in 8-oxo-DG+/PV+ cells shown in Fig. 2e indicates an effect of light vs. dark phase ( $p < 0.0001$ ) as well as an effect of ZT ( $p < 0.0001$ ). The intensity of 8-oxo-dG in PV cells was reduced at all ZTs relative to ZT0 ( $p < 0.0001$  for all ZTs). We then compared the intensity of 8-oxo-dG+/WFA+ vs. 8-oxo-dG+/PV+ cells (Fig. 2f). There was a main effect of cell subtype ( $F_{1,3299} = 23.9$ ,  $p < 0.0001$ ), a main effect of ZT ( $F_{2,3299} = 12.4$ ,  $p < 0.0001$ ), and a cell subtype x ZT interaction ( $F_{1,3299} = 15.7$ ,  $p < 0.0001$ ), with greater increases in 8-oxo-dG intensity in PV+ containing cells compared with WFA+ containing cells. Therefore, a major determinant of 8-oxo-dG buildup was the PV cell phenotype rather than the presence of PNNs.

We analyzed whether the magnitude of 8-oxo-dG intensity was associated with WFA or PV intensity. We conducted a median-split analysis of 8-oxo-dG intensity for all ZTs combined, dividing 8-oxo-dG into low or high intensity. We then examined whether WFA intensity (expressed as percent of its own ZT0, as before) was different in the low- vs. high-intensity 8-oxo-dG-containing cells. WFA intensity in low-intensity cells was  $97.2 \pm 2.5\%$  and in high-intensity cells was  $137.0 \pm 4.5\%$  ( $p < 0.0001$ ). PV intensity in low-intensity 8-oxo-dG cells was  $64.7 \pm 1.9\%$  and in high-intensity cells was  $95 \pm 2.4\%$  ( $p$

< 0.0001). Therefore, in 8-oxo-dG+/PV+/WFA+ cells, both WFA intensity and PV intensity were higher in cells with high 8-oxo-dG intensity than in cells with low 8-oxo-dG intensity.

We also examined the number and percent of 8-oxo-dG+ single, double, and triple-labeled cells (Table 2). There was an effect of ZT only for 8-oxo-dG+/PV+ double-labeled cells ( $p = 0.007$ ), with a decrease of approximately 50% at ZT6 ( $p = 0.008$ ) and a decrease of approximately 40% at ZT12 ( $p = 0.037$ ). There was also an effect of ZT for 8-oxo-dG+/WFA+/PV+ triple-labeled cells ( $p = 0.021$ ), with a decrease of approximately 60% at ZT6 relative to ZT0 ( $p = 0.015$ ). For the percent of 8-oxo-dG double- and triple-labeled cells, only 5-9% of these cells contained either WFA or PV, and about 2-4% contained both WFA and PV. The vast majority of WFA+ cells contained 8-oxo-dG (86-92%), and, as with WFA+ single-labeled cells, there was an effect of light vs. dark phase for the percent of WFA+ cells positive for 8-oxo-dG ( $p = 0.010$ ). Similarly, most WFA+/PV+ neurons also contained 8-oxo-dG (93-96%). In contrast, only 56-59% of PV+ cells contained 8-oxo-dG, suggesting that there was a substantial (40%) population of PV neurons that may be much less metabolically active compared with those surrounded by PNNs or in which 8-oxo-dG was too low to be detected in our system. Overall, these results indicate that oxidative stress levels, as indicated by 8-oxo-dG levels, is highest in PV+ cells, and the diurnal decrease in 8-oxo-dG levels at ZT6 and ZT12 is larger in non-PV+ cells compared with PV+ cells.

#### *Diurnal fluctuation of excitatory puncta in WFA+/PV+ cells at ZT6 vs. ZT18*

We observed the largest differences in intensity of WFA+/PV+ staining between ZT6 and ZT18 and therefore chose these two time points to further test whether there were diurnal differences in inhibitory and excitatory inputs to these cells. Fig. 3a and 3b show a representative PV neuron surrounded by a WFA-labeled PNN and apposed by GAD65/67-labeled inhibitory and vGLUT1-labeled excitatory puncta. While the number of GAD65/67 puncta was not different between ZT6 and ZT18 (Fig. 3c), the number of vGLUT1 puncta was increased at ZT18

compared with ZT6 ( $p = 0.0075$ ; Fig. 3d). There was a strong trend for a decreased ratio of GAD65/67:vGLUT1 at ZT18 compared with ZT6 ( $p = 0.0529$ ; Fig. 3e) and a small but significant increase in the volume of the rendered surface through the middle of the analyzed WFA+/PV+ cells ( $p = 0.0236$ ; Fig. 3f).

We also measured the number of GAD65/67 and vGLUT1 puncta apposing PV cells devoid of PNNs (WFA-/PV+ cells) to determine whether there were diurnal differences similar to those found in PNN-surrounded PV cells. Fig. 3g-j show that there were no differences in inhibitory or excitatory puncta or in the volume of WFA-/PV+ cells. The volume of WFA+/PV+ cells was significantly larger than WFA-/PV+ cells (WFA+ effect  $F_{1,76} = 16.79$ ;  $p < 0.0001$ ), as previously reported for humans (Enwright et al. 2016), and the volume of PV cells was positively correlated with PNN intensity ( $p = 0.0237$ ; data not shown). Overall, these findings suggest that PV cell volume and diurnal changes in excitatory puncta are dependent on the presence of PNNs.

#### *Diurnal fluctuation of AMPA:NMDA ratio in WFA+/PV+ cells at ZT6 vs. ZT18*

To determine whether there may also be post-synaptic changes in excitatory transmission at ZT6 and ZT18 we measured the AMPA:NMDA ratio in WFA+ fast-spiking interneurons at these two time points. The fast-spiking interneurons in this region of the cortex are highly likely to be PV-containing cells (Kawaguchi and Kubota 1993). Fig. 4a shows a representative trace of the amplitudes from AMPA- and NMDA-mediated currents. The individual amplitudes for AMPA EPSCs were greater at ZT18 compared with ZT6, and the AMPA:NMDA ratio of WFA+/PV+ cells shown in Fig. 4b increased at ZT18 compared with ZT6 (ZT6  $N = 7$ :  $0.55 \pm 0.05$ ; ZT18  $N = 8$ :  $0.91 \pm 0.13$ ,  $p = 0.0347$ ). This increase in AMPA:NMDA ratio could be due to increased calcium-permeable (CP)-AMPA utilization, decreased NMDA-mediated transmission, or a combination of both. Additionally, we observed an apparent difference in the slopes of the isolated NMDAR current (Fig. 4a, green traces). Further evaluation of NMDAR decay kinetics

shown in Fig. 4c revealed only a weak trend toward an increase in the time constant at ZT18 compared with ZT6 (ZT6 N = 7, 41.63 ms  $\pm$  6.27; ZT18 N = 8, 54.74 ms  $\pm$  4.12,  $p$  = 0.0965). An increase in the time constant would be a common indicator of a shift in subunit composition from GluN2A (highly expressed on PV+ fast-spiking cells) to GluN2B.

#### *Number of OTX2+ cells at ZT6 vs. ZT18*

Because OTX2 is necessary to maintain PNNs (Beurdeley et al. 2012; Miyata et al. 2012; Bernard and Prochiantz 2016; Sugiyama et al. 2008), we also determined whether there was a diurnal difference in the number of WFA+/PV+ cells double- or triple-labeled with OTX2 between ZT6 and ZT18. Fig. 5a shows a region of mPFC containing single-, double-, and triple-labeled OTX2+ cells. Fig. 5b and 5c show that there were no differences across timepoints in the total number of cells labeled with OTX2+ or in number of OTX2+/WFA+ cells, whereas Fig. 5d and 5e show that there was a strong trend for an increased number of double-labeled OTX2+/PV+ cells ( $p$  = 0.0609) and triple-labeled OTX2+/WFA+/PV+ cells ( $p$  = 0.0770). Interestingly, the number of PV cells that did not co-label with OTX2+ was not different between ZT6 and ZT18 ( $p$  = 0.1936), suggesting that PV+/OTX2- cells may constitute a different PV phenotype that is not regulated diurnally.

The number of OTX2+ single-, double-, and triple-labeled cells and the percent of co-labeled cells was also determined (Table 3). There were no other changes in the number of these cells between ZT6 and ZT18 beyond those shown in Fig. 5. Approximately 20% of OTX2+ cells were co-labeled with WFA, whereas only about 10% of OTX2+ cells were co-labeled with PV, and about 7% were co-labeled with both WFA and PV. The majority of cells staining for WFA or PV or both WFA and PV were co-labeled with OTX2 (ranging from 67-94%). Overall, these findings indicate that OTX2 is not limited to a single PV-containing phenotype, and the number of OTX2 cells co-labeled with PV or WFA/PV trends toward an increase at ZT18 vs. ZT6.

## DISCUSSION

Here we report several novel findings regarding diurnal variations in the biochemical features and physiology of PV cells and PNNs: 1) the intensities of biochemical markers for PV cells and PNNs in the mPFC increased during the dark, active period; 2) the oxidative stress marker, 8-oxo-dG, decreased across all time points relative to ZT0, with decreases most pronounced in non-PV-containing cells; 3) the increase in PV and PNN intensity at ZT18 were accompanied by an increase in excitatory (vGLUT1) puncta in PV cells surrounded by PNNs and, in parallel with this finding, 4) the AMPA:NMDA ratio was increased in PV/PNN cells; and 5) the number of cells co-labeled for PV/OTX2 and PV/WFA/OTX2 trended toward increases at ZT18 relative to ZT6.

### ***PNN intensity is increased in the dark phase***

The intensity of PNNs was higher in the dark phase (ZT12, ZT18) compared with the light phase (ZT0, ZT6). Diurnal fluctuation in the number of WFA-labeled PNNs has recently been reported for mice and humans (Pantazopoulos et al. 2020). The study in mice revealed that the number of PNNs in several brain regions, including in the mPFC, followed a diurnal pattern, with higher numbers of PNNs in the dark, active phase. PNN-surrounded neurons in mPFC also demonstrated a similar diurnal pattern when mice were held under conditions of constant darkness, indicating the presence of a true circadian rhythm (Pantazopoulos et al. 2020). A circadian contribution (vs. sleep contribution) to the diurnal rhythm is consistent with the minimal changes in PNN intensity we previously observed at ZT6 after 6 hr sleep disruption (Harkness et al. 2019). In contrast to the Pantazopoulos study in mice (Pantazopoulos et al. 2020), we found no diurnal rhythm in the *number* of WFA-labeled PNNs but instead a diurnal rhythm in the *intensity* of PNNs, suggesting that perhaps very dim PNNs were not visible in the mouse study or that there are species differences in PNN expression. Importantly, the intensity of PNNs

influences the extent of plasticity of their underlying neurons, based on studies in knockout mice missing a critical proteoglycan for PNN formation (link protein 1); these mice have much less intense PNNs yet exhibit delayed critical period plasticity in the visual cortex (Carulli et al. 2010). In studies in which PNNs are removed by Ch-ABC, decreased intensity of PNNs in the light phase would be expected to impart an increase in membrane capacitance (Tewari et al. 2018), a decrease in firing rate (Tewari et al. 2018; Dityatev et al. 2007; Balmer 2016), a lower resting membrane potential (Morawski et al. 2015) and changes in ion mobility around PV cells, including  $\text{Ca}^{2+}$  (Hrabetova et al. 2009; Hartig et al. 1999). Thus, an increase in PNN intensity during the active phase may allow for underlying neurons to maintain high firing rates when sleep is less likely to occur, since removal of PNNs decreases the firing rate of PV neurons. In turn, a decrease in PNN intensity in the inactive phase may promote high plasticity during sleep in the light phase, leading to stabilization or removal of synapses needed for memory consolidation (Tononi and Cirelli 2003, 2014; Rasch and Born 2013; Seibt and Frank 2019).

The particular component(s) of PNNs that are diurnally regulated is unknown. The daily decrease in PNNs appears to be regulated at least in part by cathepsin-S in the mPFC (Pantazopoulos et al. 2020). Pantazopoulos *et al.* (Pantazopoulos et al. 2020) recently suggested that circadian changes in the number of PNNs may be related to changes in the sulfation pattern on chondroitin sulfate proteoglycans of PNNs (Pantazopoulos et al. 2020), since it is difficult to conceive that the entirety of PNNs would fluctuate diurnally. Two key sulfation patterns on chondroitin sulfate chains attached to proteoglycans in PNNs are the 4-sulfation and 6-sulfation pattern, with 4-sulfation chondroitin sulfate chains prevalent in adults (Carulli et al. 2010; Miyata et al. 2012). WFA appears to bind to the 4-sulfated chains on aggrecan (Miyata and Kitagawa 2016; Giamanco et al. 2010), suggesting that aggrecan or sulfation patterns on aggrecan may be reduced during the light period and restored during the more active dark period. But how these changes would occur on a rapid, daily basis is unknown.



The composition of chondroitin sulfate chains is central to regulating plasticity because these chains form binding sites for several molecules on PNNs, including semaphorin 3A (Carulli et al. 2013), neuronal-activity regulated pentraxin 2 (Nptx2), (Van't Spijker et al. 2019), which clusters AMPARs on PV neurons (Pelkey et al. 2015), and the transcription factor OTX2 (Sugiyama et al. 2008; Beurdeley et al. 2012; Miyata et al. 2012); all of these molecules regulate plasticity.

### ***OTX2 expression in the light vs. dark phase***

We examined whether there was diurnal expression of OTX2, which is synthesized in the choroid plexus (Spatazza et al. 2013), binds to PNNs (Beurdeley et al. 2012), and is internalized within PNN-surrounded cells where it acts as a transcription factor (Beurdeley et al. 2012; Bernard and Prochiantz 2016). OTX2 is transferred to PV cells in the visual cortex and is responsible for both opening and closing the critical period of plasticity in part through its binding to PNNs (Beurdeley et al. 2012; Sugiyama et al. 2008). In the prelimbic mPFC, about 20% of OTX2-containing cells co-expressed PNNs (Table 3). Unlike in the visual cortex (Beurdeley et al. 2012), OTX2 in the mPFC is not preferentially accumulated by WFA+ or PV+ cells ((Lee et al. 2017); this study). On the other hand, the majority of single-labeled WFA+ cells, PV+ cells, and double-labeled WFA+/PV+ cells contained OTX2. While we found no diurnal difference in the *total* number of cells expressing OTX2, we did observe a strong trend toward diurnal rhythmicity in both the number of *PV+ cells* and *WFA+/PV+ cells* containing OTX2 (Figure 5; Table 3). This finding suggests that OTX2 may accumulate specifically in PV+ cells in a diurnal-dependent manner to upregulate PV and PNNs and in turn regulate excitatory:inhibitory balance. Diurnal expression of *OTX2* mRNA has been demonstrated in the rat pineal gland, with maximal expression in the dark phase (Rohde et al. 2014). OTX2 has been suggested to reciprocally interact with CLOCK in a positive regulatory loop in *Xenopus* embryos (Green et al. 2001), and analysis of OTX2-dependent critical period gene expression identified upregulation of *Per1* in mouse visual cortex (Apulei et al. 2019).

OTX2 regulates several PNN components in the mPFC, possibly by altering turnover of these components (Lee et al. 2017). Several downstream targets of OTX2 have been identified, including the GluN2A subunit of the NMDA receptor (see below), and the antioxidant gene oxidation resistance 1 (*Oxr1*), whose gene product acts as a sensor of oxidative stress and is enriched in GABAergic neurons in the visual cortex (Sakai et al. 2017). OTX2 also may bind to several potassium channel genes, including the Kv3.1 family, a key ion channel that maintains fast spiking in PV cells (Du et al. 1996). Thus, diurnal expression of OTX2 likely coordinates the expression of several important genes in PV cells to render these neurons responsive to external signals (Sakai et al. 2017) and oxidative stress to support daily fluctuation of firing rates and gamma oscillations needed to provide appropriate excitatory:inhibitory balance during sleep and wakefulness (Gronli et al. 2016).

***PV cell intensity, excitatory puncta, and AMPA:NMDA ratio are increased in the dark phase***

We also demonstrated diurnal rhythmicity of PV expression in mPFC cells. PV protein levels have shown a circadian pattern of expression in retinal amacrine cells, with higher expression in the dark, active phase (Gabriel et al. 2004). Expression of PV is regulated by *Clock* gene expression in the visual cortex (Kobayashi et al. 2015). Thus, similar CLOCK-dependent rhythms of PV levels may occur in the prelimbic mPFC. Diurnal changes in PV intensity have been shown to be positively correlated with GAD67 intensity (Donato et al. 2013) and likely reflect activity levels needed to sustain homeostatic balance for excitatory:inhibitory output. Parvalbumin is a  $\text{Ca}^{2+}$  buffering protein (Celio 1990), which may lead to multi-faceted consequences of diurnal variation in PV levels. For example, low expression of PV in the absence of prolonged bursts of action potentials may promote short-term plasticity through facilitation (Caillard et al. 2000; Eggermann and Jonas 2011), while high expression of PV may

lower the release probability of GABA by acting as a fast  $\text{Ca}^{2+}$  buffer (Eggermann and Jonas 2011). Low PV levels may therefore function to amplify low-input signals, whereas high PV levels may function as a high-pass filter to dampen low-input signals. High PV levels may also act as a brake on excitation-transcription coupling *via* a cAMP response element-binding protein (CREB)-dependent process (Cohen et al. 2016), which in turn regulates several genes (Impey et al. 2004) that could orchestrate day/night fluctuations in PV cell function.

In concert with increases in PV levels during the dark phase, we found two additional diurnal changes consistent with increases in glutamate transmission at ZT18. First, the AMPA:NMDA ratio was increased in WFA+/PV+ cells at ZT18 relative to ZT6, which may drive a higher cell firing rate. Previous observations in neurons of the cerebral cortex indicated that protracted wakefulness upregulates AMPA receptor-mediated signaling (Vyazovskiy et al. 2008), but the neurochemical phenotype of these neurons is unknown. Therefore, the increase in AMPA/NMDA ratio we observed at ZT18 (a time when rats have been awake for several hours after dark onset) may be driven by sustained wakefulness rather than an endogenous circadian oscillator. In PV cells, AMPA receptors have an abundance of GluA1 and GluA4 subunits, making them calcium permeable (Akgul and McBain 2016), which contributes to faster kinetic properties, including higher single-channel conductance and faster gating properties compared with GluA2-containing AMPARs (Akgul and McBain 2016; Swanson et al. 1997). Second, we observed an increase in the number of vGLUT1 synaptic puncta apposing WFA+/PV+ cells at ZT18 relative to ZT6 (Fig. 3). Interestingly, we found no changes in vGLUT1 puncta apposing PV+ cells *devoid* of PNNs (WFA-/PV+ cells), suggesting that the presumed higher firing rate of PV cells with PNNs vs. those without PNNs may contribute to maintaining diurnal fluctuation in excitatory:inhibitory balance. It is also possible that NMDARs are altered diurnally. Our recordings demonstrated that the NMDA current was greater than the AMPA current. There is an early switch during postnatal development from GluN2B to GluN2A expression (Zhang and

Sun 2011), and PV function is maintained by GluN2A-containing NMDA receptors (Kinney et al. 2006). The trend toward a slower time constant in PV+/WFA+ cells at ZT18 suggests that the NMDA component is more NR2B dominant, as slower time constants indicate a shift from GluN2A to GluN2B composition (Brown et al. 2011). Future experiments are needed to determine the extent of diurnal rhythm-induced compositional changes in NMDA receptors. Overall, our findings indicate that glutamate transmission is high during the active phase at ZT18 relative to the inactive phase at ZT6. The reduction in PNN intensity during the inactive phase may lead to lower CP-AMPA receptors in part *via* reduced accumulation of Nptx2 within PNN-surrounded PV cells (Chang et al. 2010). Collectively, these changes may help coordinate not only excitatory:inhibitory balance needed for pyramidal cell output during wakefulness, but also for homeosynaptic scaling during sleep to restore synaptic homeostasis (Tononi and Cirelli 2014). Importantly, most rodent studies are conducted in the daytime phase, and thus modulation of PV cell electrophysiology and transcription-coupling by factors such as glutamatergic input that regulates pCREB in pyramidal cells but not in PV cells (Cohen et al. 2016) might be unveiled if PV cells were tested during the dark phase.

### ***Oxidative stress is highest at ZT0 and remains higher in PV vs. non-PV cells***

Diurnal changes in oxidative stress are observed in a multitude of studies, demonstrated by fluctuations in the extent of DNA damage, lipid peroxidation, and protein oxidation (Wilking et al. 2013; Kanabrocki et al. 2002). These downstream effects appear to be initiated by the impact of accumulated reactive oxygen species (ROS) (Wilking et al. 2013; Gupta and Ragsdale 2011). The diurnal oscillation we observed in the oxidative stress marker 8-oxo-dG aligns with our previous findings (Harkness et al. 2019) and previous studies (Silva et al. 2004; Ramanathan et al. 2010) that oxidative stress accumulates in rodent brains during wakefulness. The diurnal changes reflect the rhythmicity of mitochondrial network remodeling and the dynamic capacity of oxidative phosphorylation, which peaks in the dark phase (Schmitt et al. 2018) during

wakefulness relative to sleep (reviewed in (Wisor 2011; Aalling et al. 2018)). Here we show that 8-oxo-dG intensity in the prelimbic mPFC was highest at ZT0 and lowest at ZT12 (Figure 2), likely reflecting clearance of 8-oxo-dG during sleep. Our previous work demonstrated that increasing the time rats spent awake due to sleep disruption contributed to increases in 8-oxo-dG intensity, especially in PV-expressing neurons (Harkness et al. 2019). The mitochondria of PV-expressing neurons in particular exhibit elevated energy demands, as these neurons are essential for generating gamma activity, which requires a high and sustained firing rate and frequency (Sohal et al. 2009), rendering PV cells especially vulnerable to oxidative stress compared with other types of neurons (Kann et al. 2014). As demonstrated here, accumulation of oxidative stress occurred even without sleep disruption, but it is likely that both sleep and circadian mechanisms contribute to the rhythmicity of ROS accumulation and damage related to oxidative stress, as explained by the two-process model (Lai et al. 2012; Borbely et al. 2016). Studying the dynamics of PNNs and PV neuronal activity from the framing of the two process-model may be helpful in understanding their variability, and examination of this is ongoing.

Both CLOCK and OTX2 appear to protect cells against the effects of oxidative stress (Kobayashi et al. 2015; Lee et al. 2017), and, as they regulate plasticity during development, they may also regulate diurnal changes. PNNs protect their underlying neurons from oxidative stress due to their enrichment in chondroitin sulfate (Campo et al. 2004), although PNNs are also subject to deleterious effects by oxidative stress (Cabungcal et al. 2013). Our findings that PNN intensity changes across the day/night cycle suggest that protective mechanisms from oxidative stress is also be subject to diurnal variation.

## **Conclusions**

Our findings indicate that PNN, PV, and 8-oxo-dG intensities fluctuate throughout the day. Increases in WFA and PV intensity precede changes in 8-oxo-dG intensity, suggesting a

circadian-regulated increase in PNNs around PV cells at the onset of the active phase, potentially in preparation for increased glutamatergic input and presumed increases in cell firing. OTX2 may serve a role in coordinating diurnal changes in gene expression needed for optimal performance of PV cell firing during sleep and wakefulness, including proteins providing protection from oxidative stress. Diurnal fluctuation in these parameters are important and thus far are largely unconsidered factors in interpretation of the impact these fluctuations may have on basic cellular functions such as electrophysiological properties and transcription-coupling mechanisms typically measured during the light phase. Furthermore, interpretation of diurnal fluctuations in PV cell function is vital for considering treatment and study of disease states impacted by sleep and circadian factors. Given the fundamental role of PV-expressing neurons in brain disorders and the maintenance of cortical excitatory:inhibitory balance and gamma oscillations necessary for attention and cognitive flexibility (Sohal et al. 2009; Cho et al. 2015; Uhlhaas and Singer 2010), it is important to establish how daily rhythmicity is coordinated among OTX2, oxidative stress, and PNN/PV function in the mPFC.

**Acknowledgements:**

The authors would like to thank Dr. Megan Slaker, Ryan P. Todd, Monica Chang, and Nathan Allen for help with earlier stages of the experiments and Jonathan Ramos for assistance with analysis.

## REFERENCES

- Aalling NN, Nedergaard M, DiNuzzo M (2018) Cerebral Metabolic Changes During Sleep. *Curr Neurol Neurosci Rep* 18 (9):57. doi:10.1007/s11910-018-0868-9
- Akgul G, McBain CJ (2016) Diverse roles for ionotropic glutamate receptors on inhibitory interneurons in developing and adult brain. *J Physiol* 594 (19):5471-5490. doi:10.1113/JP271764
- Apulei J, Kim N, Testa D, Ribot J, Morizet D, Bernard C, Jourdain L, Blugeon C, Di Nardo AA, Prochiantz A (2019) Non-cell Autonomous OTX2 Homeoprotein Regulates Visual Cortex Plasticity Through Gadd45b/g. *Cereb Cortex* 29 (6):2384-2395. doi:10.1093/cercor/bhy108
- Balmer TS (2016) Perineuronal Nets Enhance the Excitability of Fast-Spiking Neurons. *eNeuro* 3 (4). doi:10.1523/ENEURO.0112-16.2016
- Balmer TS, Carels VM, Frisch JL, Nick TA (2009) Modulation of perineuronal nets and parvalbumin with developmental song learning. *The Journal of neuroscience* 29 (41):12878-12885
- Bernard C, Prochiantz A (2016) Otx2-PNN Interaction to Regulate Cortical Plasticity. *Neural Plast* 2016:7931693. doi:10.1155/2016/7931693
- Beurdeley M, Spatazza J, Lee HH, Sugiyama S, Bernard C, Di Nardo AA, Hensch TK, Prochiantz A (2012) Otx2 binding to perineuronal nets persistently regulates plasticity in the mature visual cortex. *J Neurosci* 32 (27):9429-9437. doi:10.1523/JNEUROSCI.0394-12.2012
- Borbely AA, Daan S, Wirz-Justice A, Deboer T (2016) The two-process model of sleep regulation: a reappraisal. *J Sleep Res* 25 (2):131-143. doi:10.1111/jsr.12371
- Braver TS, Cohen JD, Nystrom LE, Jonides J, Smith EE, Noll DC (1997) A parametric study of prefrontal cortex involvement in human working memory. *Neuroimage* 5 (1):49-62. doi:10.1006/nimg.1996.0247
- Brown TE, Lee BR, Mu P, Ferguson D, Dietz D, Ohnishi YN, Lin Y, Suska A, Ishikawa M, Huang YH, Shen H, Kalivas PW, Sorg BA, Zukin RS, Nestler EJ, Dong Y, Schluter OM (2011) A silent synapse-based mechanism for cocaine-induced locomotor sensitization. *J Neurosci* 31 (22):8163-8174. doi:10.1523/JNEUROSCI.0016-11.2011
- Bruckner G, Brauer K, Hartig W, Wolff JR, Rickmann MJ, Derouiche A, Delpech B, Girard N, Oertel WH, Reichenbach A (1993) Perineuronal nets provide a polyanionic, glia-associated form of microenvironment around certain neurons in many parts of the rat brain. *Glia* 8 (3):183-200. doi:10.1002/glia.440080306
- Buzsaki G, Draguhn A (2004) Neuronal oscillations in cortical networks. *Science* 304 (5679):1926-1929. doi:10.1126/science.1099745
- Cabungcal JH, Steullet P, Morishita H, Kraftsik R, Cuenod M, Hensch TK, Do KQ (2013) Perineuronal nets protect fast-spiking interneurons against oxidative stress. *Proc Natl Acad Sci U S A* 110 (22):9130-9135. doi:10.1073/pnas.1300454110
- Caillard O, Moreno H, Schwaller B, Llano I, Celio MR, Marty A (2000) Role of the calcium-binding protein parvalbumin in short-term synaptic plasticity. *Proc Natl Acad Sci U S A* 97 (24):13372-13377. doi:10.1073/pnas.230362997
- Campo GM, Avenoso A, Campo S, D'Ascola A, Ferlazzo AM, Calatroni A (2004) Reduction of DNA fragmentation and hydroxyl radical production by hyaluronic acid and chondroitin-4-sulphate in iron plus ascorbate-induced oxidative stress in fibroblast cultures. *Free Radic Res* 38 (6):601-611. doi:10.1080/10715760410001694017
- Cardin JA, Carlen M, Meletis K, Knoblich U, Zhang F, Deisseroth K, Tsai LH, Moore CI (2009) Driving fast-spiking cells induces gamma rhythm and controls sensory responses. *Nature* 459 (7247):663-667. doi:10.1038/nature08002

- Carmassi C, Palagini L, Caruso D, Masci I, Nobili L, Vita A, Dell'Osso L (2019) Systematic Review of Sleep Disturbances and Circadian Sleep Desynchronization in Autism Spectrum Disorder: Toward an Integrative Model of a Self-Reinforcing Loop. *Front Psychiatry* 10:366. doi:10.3389/fpsy.2019.00366
- Carulli D, Foscarin S, Faralli A, Pajaj E, Rossi F (2013) Modulation of semaphorin3A in perineuronal nets during structural plasticity in the adult cerebellum. *Mol Cell Neurosci* 57:10-22. doi:10.1016/j.mcn.2013.08.003
- Carulli D, Pizzorusso T, Kwok JC, Putignano E, Poli A, Forostyak S, Andrews MR, Deepa SS, Glant TT, Fawcett JW (2010) Animals lacking link protein have attenuated perineuronal nets and persistent plasticity. *Brain* 133 (8):2331-2347
- Celio MR (1990) Calbindin D-28k and parvalbumin in the rat nervous system. *Neuroscience* 35 (2):375-475. doi:10.1016/0306-4522(90)90091-h
- Chakravorty S, Vandrey RG, He S, Stein MD (2018) Sleep Management Among Patients with Substance Use Disorders. *Med Clin North Am* 102 (4):733-743. doi:10.1016/j.mcna.2018.02.012
- Chang MC, Park JM, Pelkey KA, Grabenstatter HL, Xu D, Linden DJ, Sutula TP, McBain CJ, Worley PF (2010) Narp regulates homeostatic scaling of excitatory synapses on parvalbumin-expressing interneurons. *Nat Neurosci* 13 (9):1090-1097. doi:10.1038/nn.2621
- Chellappa SL, Gaggioni G, Ly JQ, Papachilleos S, Borsu C, Brzozowski A, Rosanova M, Sarasso S, Luxen A, Middleton B, Archer SN, Dijk DJ, Massimini M, Maquet P, Phillips C, Moran RJ, Vandewalle G (2016) Circadian dynamics in measures of cortical excitation and inhibition balance. *Sci Rep* 6:33661. doi:10.1038/srep33661
- Cho KK, Hoch R, Lee AT, Patel T, Rubenstein JL, Sohal VS (2015) Gamma rhythms link prefrontal interneuron dysfunction with cognitive inflexibility in *Dlx5/6*(+/-) mice. *Neuron* 85 (6):1332-1343. doi:10.1016/j.neuron.2015.02.019
- Cohen SM, Ma H, Kuchibhotla KV, Watson BO, Buzsaki G, Froemke RC, Tsien RW (2016) Excitation-Transcription Coupling in Parvalbumin-Positive Interneurons Employs a Novel CaM Kinase-Dependent Pathway Distinct from Excitatory Neurons. *Neuron* 90 (2):292-307. doi:10.1016/j.neuron.2016.03.001
- Di Nardo AA, Fuchs J, Joshi RL, Moya KL, Prochiantz A (2018) The Physiology of Homeoprotein Transduction. *Physiol Rev* 98 (4):1943-1982. doi:10.1152/physrev.00018.2017
- Dingess PM, Darling RA, Derman RC, Wulff SS, Hunter ML, Ferrario CR, Brown TE (2017) Structural and Functional Plasticity within the Nucleus Accumbens and Prefrontal Cortex Associated with Time-Dependent Increases in Food Cue-Seeking Behavior. *Neuropsychopharmacology* 42 (12):2354-2364. doi:10.1038/npp.2017.57
- Dityatev A, Bruckner G, Dityateva G, Grosche J, Kleene R, Schachner M (2007) Activity-dependent formation and functions of chondroitin sulfate-rich extracellular matrix of perineuronal nets. *Dev Neurobiol* 67 (5):570-588. doi:10.1002/dneu.20361
- Donato F, Rompani SB, Caroni P (2013) Parvalbumin-expressing basket-cell network plasticity induced by experience regulates adult learning. *Nature* 504 (7479):272-276. doi:10.1038/nature12866
- Du J, Zhang L, Weiser M, Rudy B, McBain CJ (1996) Developmental expression and functional characterization of the potassium-channel subunit Kv3.1b in parvalbumin-containing interneurons of the rat hippocampus. *J Neurosci* 16 (2):506-518
- Eggermann E, Jonas P (2011) How the 'slow' Ca(2+) buffer parvalbumin affects transmitter release in nanodomain-coupling regimes. *Nat Neurosci* 15 (1):20-22. doi:10.1038/nn.3002
- Elvevag B, Goldberg TE (2000) Cognitive impairment in schizophrenia is the core of the disorder. *Crit Rev Neurobiol* 14 (1):1-21



- Enwright JF, Sanapala S, Foglio A, Berry R, Fish KN, Lewis DA (2016) Reduced Labeling of Parvalbumin Neurons and Perineuronal Nets in the Dorsolateral Prefrontal Cortex of Subjects with Schizophrenia. *Neuropsychopharmacology* 41 (9):2206-2214. doi:10.1038/npp.2016.24
- Fanjul-Moles ML, Lopez-Riquelme GO (2016) Relationship between Oxidative Stress, Circadian Rhythms, and AMD. *Oxid Med Cell Longev* 2016:7420637. doi:10.1155/2016/7420637
- Fawcett JW, Ohashi T, Pizzorusso T (2019) The roles of perineuronal nets and the perinodal extracellular matrix in neuronal function. *Nat Rev Neurosci* 20 (8):451-465. doi:10.1038/s41583-019-0196-3
- Ferguson BR, Gao WJ (2018a) PV Interneurons: Critical Regulators of E/I Balance for Prefrontal Cortex-Dependent Behavior and Psychiatric Disorders. *Frontiers in neural circuits* 12:37. doi:10.3389/fncir.2018.00037
- Ferguson BR, Gao WJ (2018b) Thalamic Control of Cognition and Social Behavior Via Regulation of Gamma-Aminobutyric Acidergic Signaling and Excitation/Inhibition Balance in the Medial Prefrontal Cortex. *Biol Psychiatry* 83 (8):657-669. doi:10.1016/j.biopsych.2017.11.033
- Foscarin S, Raha-Chowdhury R, Fawcett JW, Kwok JCF (2017) Brain ageing changes proteoglycan sulfation, rendering perineuronal nets more inhibitory. *Aging (Albany NY)* 9 (6):1607-1622. doi:10.18632/aging.101256
- Gabriel R, Lesauter J, Banvolgyi T, Petrovics G, Silver R, Witkovsky P (2004) All amacrine neurons of the rat retina show diurnal and circadian rhythms of parvalbumin immunoreactivity. *Cell Tissue Res* 315 (2):181-186. doi:10.1007/s00441-003-0785-2
- Giamanco KA, Morawski M, Matthews RT (2010) Perineuronal net formation and structure in aggrecan knockout mice. *Neuroscience* 170 (4):1314-1327. doi:S0306-4522(10)01160-7 [pii] 10.1016/j.neuroscience.2010.08.032
- Gogolla N, Caroni P, Luthi A, Herry C (2009) Perineuronal nets protect fear memories from erasure. *Science* 325 (5945):1258-1261. doi:325/5945/1258 [pii] 10.1126/science.1174146
- Goldman-Rakic PS (1994) Working memory dysfunction in schizophrenia. *J Neuropsychiatry Clin Neurosci* 6 (4):348-357. doi:10.1176/jnp.6.4.348
- Goldstein RZ, Craig AD, Bechara A, Garavan H, Childress AR, Paulus MP, Volkow ND (2009) The neurocircuitry of impaired insight in drug addiction. *Trends Cogn Sci* 13 (9):372-380. doi:10.1016/j.tics.2009.06.004
- Green CB, Durston AJ, Morgan R (2001) The circadian gene Clock is restricted to the anterior neural plate early in development and is regulated by the neural inducer noggin and the transcription factor Otx2. *Mech Dev* 101 (1-2):105-110. doi:10.1016/s0925-4773(00)00559-1
- Green MJ, Girshkin L, Kremerskothen K, Watkeys O, Quide Y (2019) A Systematic Review of Studies Reporting Data-Driven Cognitive Subtypes across the Psychosis Spectrum. *Neuropsychol Rev*. doi:10.1007/s11065-019-09422-7
- Gronli J, Rempe MJ, Clegern WC, Schmidt M, Wisor JP (2016) Beta EEG reflects sensory processing in active wakefulness and homeostatic sleep drive in quiet wakefulness. *J Sleep Res* 25 (3):257-268. doi:10.1111/jsr.12380
- Gupta N, Ragsdale SW (2011) Thiol-disulfide redox dependence of heme binding and heme ligand switching in nuclear hormone receptor rev-erb $\beta$ . *J Biol Chem* 286 (6):4392-4403. doi:10.1074/jbc.M110.193466
- Harkness JH, Bushana PN, Todd RP, Clegern WC, Sorg BA, Wisor JP (2019) Sleep disruption elevates oxidative stress in parvalbumin-positive cells of the rat cerebral cortex. *Sleep* 42 (1). doi:10.1093/sleep/zsy201
- Hartig W, Brauer K, Bruckner G (1992) Wisteria floribunda agglutinin-labelled nets surround parvalbumin-containing neurons. *Neuroreport* 3 (10):869-872

- Hartig W, Derouiche A, Welt K, Brauer K, Grosche J, Mader M, Reichenbach A, Bruckner G (1999) Cortical neurons immunoreactive for the potassium channel Kv3.1b subunit are predominantly surrounded by perineuronal nets presumed as a buffering system for cations. *Brain Res* 842 (1):15-29. doi:S0006-8993(99)01784-9 [pii]
- Hegarty DM, Hermes SM, Largent-Milnes TM, Aicher SA (2014) Capsaicin-responsive corneal afferents do not contain TRPV1 at their central terminals in trigeminal nucleus caudalis in rats. *J Chem Neuroanat* 61-62:1-12. doi:10.1016/j.jchemneu.2014.06.006
- Hegarty DM, Tonsfeldt K, Hermes SM, Helfand H, Aicher SA (2010) Differential localization of vesicular glutamate transporters and peptides in corneal afferents to trigeminal nucleus caudalis. *J Comp Neurol* 518 (17):3557-3569. doi:10.1002/cne.22414
- Holmes GL (2015) Cognitive impairment in epilepsy: the role of network abnormalities. *Epileptic Disord* 17 (2):101-116. doi:10.1684/epd.2015.0739
- Hood S, Amir S (2017) The aging clock: circadian rhythms and later life. *J Clin Invest* 127 (2):437-446. doi:10.1172/JCI90328
- Howard MW, Rizzuto DS, Caplan JB, Madsen JR, Lisman J, Aschenbrenner-Scheibe R, Schulze-Bonhage A, Kahana MJ (2003) Gamma oscillations correlate with working memory load in humans. *Cereb Cortex* 13 (12):1369-1374. doi:10.1093/cercor/bhg084
- Hrabetova S, Masri D, Tao L, Xiao F, Nicholson C (2009) Calcium diffusion enhanced after cleavage of negatively charged components of brain extracellular matrix by chondroitinase ABC. *J Physiol* 587 (Pt 16):4029-4049. doi:10.1113/jphysiol.2009.170092
- Huber R, Maki H, Rosanova M, Casarotto S, Canali P, Casali AG, Tononi G, Massimini M (2013) Human cortical excitability increases with time awake. *Cereb Cortex* 23 (2):332-338. doi:10.1093/cercor/bhs014
- Impey S, McCorkle SR, Cha-Molstad H, Dwyer JM, Yochum GS, Boss JM, McWeeney S, Dunn JJ, Mandel G, Goodman RH (2004) Defining the CREB regulon: a genome-wide analysis of transcription factor regulatory regions. *Cell* 119 (7):1041-1054. doi:10.1016/j.cell.2004.10.032
- Jorgensen ET, Gonzalez AE, Harkness JH, Hegarty DM, Thakar A, Burchi DJ, Aadland JA, Aicher SA, Sorg BA, Brown TE (2020) Cocaine memory reactivation induces functional adaptations within parvalbumin interneurons in the rat medial prefrontal cortex. *Addict Biol*:e12947. doi:10.1111/adb.12947
- Kanabrocki EL, Murray D, Hermida RC, Scott GS, Bremner WF, Ryan MD, Ayala DE, Third JL, Shirazi P, Nemchausky BA, Hooper DC (2002) Circadian variation in oxidative stress markers in healthy and type II diabetic men. *Chronobiol Int* 19 (2):423-439. doi:10.1081/cbi-120002914
- Kann O, Papageorgiou IE, Draguhn A (2014) Highly energized inhibitory interneurons are a central element for information processing in cortical networks. *J Cereb Blood Flow Metab* 34 (8):1270-1282. doi:10.1038/jcbfm.2014.104
- Kawaguchi Y, Kubota Y (1993) Correlation of physiological subgroupings of nonpyramidal cells with parvalbumin- and calbindinD28k-immunoreactive neurons in layer V of rat frontal cortex. *J Neurophysiol* 70 (1):387-396. doi:10.1152/jn.1993.70.1.387
- Khan S, Nobili L, Khatami R, Loddenkemper T, Cajochen C, Dijk DJ, Eriksson SH (2018) Circadian rhythm and epilepsy. *Lancet Neurol* 17 (12):1098-1108. doi:10.1016/S1474-4422(18)30335-1
- Kinney JW, Davis CN, Tabarean I, Conti B, Bartfai T, Behrens MM (2006) A specific role for NR2A-containing NMDA receptors in the maintenance of parvalbumin and GAD67 immunoreactivity in cultured interneurons. *J Neurosci* 26 (5):1604-1615. doi:10.1523/JNEUROSCI.4722-05.2006
- Kobayashi Y, Ye Z, Hensch TK (2015) Clock genes control cortical critical period timing. *Neuron* 86 (1):264-275. doi:10.1016/j.neuron.2015.02.036

- Kolb B, Nonneman AJ, Singh RK (1974) Double dissociation of spatial impairments and perseveration following selective prefrontal lesions in rats. *J Comp Physiol Psychol* 87 (4):772-780. doi:10.1037/h0036970
- Lai AG, Doherty CJ, Mueller-Roeber B, Kay SA, Schippers JH, Dijkwel PP (2012) CIRCADIAN CLOCK-ASSOCIATED 1 regulates ROS homeostasis and oxidative stress responses. *Proc Natl Acad Sci U S A* 109 (42):17129-17134. doi:10.1073/pnas.1209148109
- Lee HHC, Bernard C, Ye Z, Acampora D, Simeone A, Prochiantz A, Di Nardo AA, Hensch TK (2017) Genetic Otx2 mis-localization delays critical period plasticity across brain regions. *Mol Psychiatry* 22 (5):785. doi:10.1038/mp.2017.83
- Lewis DA (2014) Inhibitory neurons in human cortical circuits: substrate for cognitive dysfunction in schizophrenia. *Curr Opin Neurobiol* 26:22-26. doi:10.1016/j.conb.2013.11.003
- Logan RW, Williams WP, 3rd, McClung CA (2014) Circadian rhythms and addiction: mechanistic insights and future directions. *Behav Neurosci* 128 (3):387-412. doi:10.1037/a0036268
- Ly JQ, Gaggioni G, Chellappa SL, Papachilleos S, Brzozowski A, Borsu C, Rosanova M, Sarasso S, Middleton B, Luxen A, Archer SN, Phillips C, Dijk DJ, Maquet P, Massimini M, Vandewalle G (2016) Circadian regulation of human cortical excitability. *Nat Commun* 7:11828. doi:10.1038/ncomms11828
- Miyata S, Kitagawa H (2016) Chondroitin sulfate and neuronal disorders. *Front Biosci (Landmark Ed)* 21:1330-1340
- Miyata S, Komatsu Y, Yoshimura Y, Taya C, Kitagawa H (2012) Persistent cortical plasticity by upregulation of chondroitin 6-sulfation. *Nat Neurosci* 15 (3):414-422, S411-412. doi:10.1038/nn.3023
- Morawski M, Reinert T, Meyer-Klaucke W, Wagner FE, Troger W, Reinert A, Jager C, Bruckner G, Arendt T (2015) Ion exchanger in the brain: Quantitative analysis of perineuronally fixed anionic binding sites suggests diffusion barriers with ion sorting properties. *Sci Rep* 5:16471. doi:10.1038/srep16471
- Murray AJ, Woloszynowska-Fraser MU, Ansel-Bollepalli L, Cole KL, Foggetti A, Crouch B, Riedel G, Wulff P (2015) Parvalbumin-positive interneurons of the prefrontal cortex support working memory and cognitive flexibility. *Sci Rep* 5:16778. doi:10.1038/srep16778
- Packer AM, Yuste R (2011) Dense, unspecific connectivity of neocortical parvalbumin-positive interneurons: a canonical microcircuit for inhibition? *J Neurosci* 31 (37):13260-13271. doi:10.1523/JNEUROSCI.3131-11.2011
- Pantazopoulos H, Berretta S (2016) In Sickness and in Health: Perineuronal Nets and Synaptic Plasticity in Psychiatric Disorders. *Neural Plast* 2016:9847696. doi:10.1155/2016/9847696
- Pantazopoulos H, Gisabella B, Rexrode L, Benefield D, Yildiz E, Seltzer P, Valeri J, Chelini G, Reich A, Ardelt M, Berretta S (2020) Circadian Rhythms of Perineuronal Net Composition. *eNeuro* 7 (4). doi:10.1523/ENEURO.0034-19.2020
- Pantazopoulos H, Wiseman JT, Markota M, Ehrenfeld L, Berretta S (2017) Decreased Numbers of Somatostatin-Expressing Neurons in the Amygdala of Subjects With Bipolar Disorder or Schizophrenia: Relationship to Circadian Rhythms. *Biol Psychiatry* 81 (6):536-547. doi:10.1016/j.biopsych.2016.04.006
- Paxinos G WC (1998) *The Rat Brain in Stereotaxic Coordinates*. 4 edn. Academic Press, New York
- Pelkey KA, Barksdale E, Craig MT, Yuan X, Sukumaran M, Vargish GA, Mitchell RM, Wyeth MS, Petralia RS, Chittajallu R, Karlsson RM, Cameron HA, Murata Y, Colonnese MT, Worley PF, McBain CJ (2015) Pentraxins coordinate excitatory synapse maturation and circuit integration of parvalbumin interneurons. *Neuron* 85 (6):1257-1272. doi:10.1016/j.neuron.2015.02.020

- Perreau-Lenz S, Spanagel R (2015) Clock genes x stress x reward interactions in alcohol and substance use disorders. *Alcohol* 49 (4):351-357. doi:10.1016/j.alcohol.2015.04.003
- Pizzorusso T, Medini P, Berardi N, Chierzi S, Fawcett JW, Maffei L (2002) Reactivation of ocular dominance plasticity in the adult visual cortex. *Science* 298 (5596):1248-1251
- Ramanathan L, Hu S, Frautschy SA, Siegel JM (2010) Short-term total sleep deprivation in the rat increases antioxidant responses in multiple brain regions without impairing spontaneous alternation behavior. *Behav Brain Res* 207 (2):305-309. doi:10.1016/j.bbr.2009.10.014
- Rankin-Gee EK, McRae PA, Baranov E, Rogers S, Wandrey L, Porter BE (2015) Perineuronal net degradation in epilepsy. *Epilepsia* 56 (7):1124-1133. doi:10.1111/epi.13026
- Rasch B, Born J (2013) About sleep's role in memory. *Physiol Rev* 93 (2):681-766. doi:10.1152/physrev.00032.2012
- Rohde K, Rovsing L, Ho AK, Moller M, Rath MF (2014) Circadian dynamics of the cone-rod homeobox (CRX) transcription factor in the rat pineal gland and its role in regulation of arylalkylamine N-acetyltransferase (AANAT). *Endocrinology* 155 (8):2966-2975. doi:10.1210/en.2014-1232
- Sakai A, Nakato R, Ling Y, Hou X, Hara N, Iijima T, Yanagawa Y, Kuwano R, Okuda S, Shirahige K, Sugiyama S (2017) Genome-Wide Target Analyses of Otx2 Homeoprotein in Postnatal Cortex. *Front Neurosci* 11:307. doi:10.3389/fnins.2017.00307
- Schmitt K, Grimm A, Dallmann R, Oettinghaus B, Restelli LM, Witzig M, Ishihara N, Mihara K, Ripperger JA, Albrecht U, Frank S, Brown SA, Eckert A (2018) Circadian Control of DRP1 Activity Regulates Mitochondrial Dynamics and Bioenergetics. *Cell Metab* 27 (3):657-666 e655. doi:10.1016/j.cmet.2018.01.011
- Seeger G, Brauer K, Hartig W, Bruckner G (1994) Mapping of perineuronal nets in the rat brain stained by colloidal iron hydroxide histochemistry and lectin cytochemistry. *Neuroscience* 58 (2):371-388
- Seibt J, Frank MG (2019) Primed to Sleep: The Dynamics of Synaptic Plasticity Across Brain States. *Front Syst Neurosci* 13:2. doi:10.3389/fnsys.2019.00002
- Seney ML, Cahill K, Enwright JF, 3rd, Logan RW, Huo Z, Zong W, Tseng G, McClung CA (2019) Diurnal rhythms in gene expression in the prefrontal cortex in schizophrenia. *Nat Commun* 10 (1):3355. doi:10.1038/s41467-019-11335-1
- Silva RH, Abilio VC, Takatsu AL, Kameda SR, Grassl C, Chehin AB, Medrano WA, Calzavara MB, Registro S, Andersen ML, Machado RB, Carvalho RC, Ribeiro Rde A, Tufik S, Frussa-Filho R (2004) Role of hippocampal oxidative stress in memory deficits induced by sleep deprivation in mice. *Neuropharmacology* 46 (6):895-903. doi:10.1016/j.neuropharm.2003.11.032
- Slaker M, Barnes J, Sorg BA, Grimm JW (2016a) Impact of Environmental Enrichment on Perineuronal Nets in the Prefrontal Cortex following Early and Late Abstinence from Sucrose Self-Administration in Rats. *PLoS One* 11 (12):e0168256. doi:10.1371/journal.pone.0168256
- Slaker M, Churchill L, Todd RP, Blacktop JM, Zuloaga DG, Raber J, Darling RA, Brown TE, Sorg BA (2015) Removal of perineuronal nets in the medial prefrontal cortex impairs the acquisition and reconsolidation of a cocaine-induced conditioned place preference memory. *J Neurosci* 35 (10):4190-4202. doi:10.1523/JNEUROSCI.3592-14.2015
- Slaker M, Harkness J and Sorg BA (2016) A standardized and automated method of perineuronal net analysis using Wisteria floribunda agglutinin staining intensity. *IBRO Reports* 1:54-60
- Slaker ML, Harkness JH, Sorg BA (2016b) A standardized and automated method of perineuronal net analysis using Wisteria floribunda agglutinin staining intensity. *IBRO Rep* 1:54-60. doi:10.1016/j.ibror.2016.10.001

- Slaker ML, Jorgensen ET, Hegarty DM, Liu X, Kong Y, Zhang F, Linhardt RJ, Brown TE, Aicher SA, Sorg BA (2018) Cocaine Exposure Modulates Perineuronal Nets and Synaptic Excitability of Fast-Spiking Interneurons in the Medial Prefrontal Cortex. *eNeuro* 5 (5). doi:10.1523/ENEURO.0221-18.2018
- Sohal VS, Zhang F, Yizhar O, Deisseroth K (2009) Parvalbumin neurons and gamma rhythms enhance cortical circuit performance. *Nature* 459 (7247):698-702. doi:nature07991 [pii] 10.1038/nature07991
- Sorg BA, Berretta S, Blacktop JM, Fawcett JW, Kitagawa H, Kwok JC, Miquel M (2016) Casting a Wide Net: Role of Perineuronal Nets in Neural Plasticity. *J Neurosci* 36 (45):11459-11468. doi:10.1523/JNEUROSCI.2351-16.2016
- Spatazza J, Lee HH, Di Nardo AA, Tibaldi L, Joliot A, Hensch TK, Prochiantz A (2013) Choroid-plexus-derived Otx2 homeoprotein constrains adult cortical plasticity. *Cell reports* 3 (6):1815-1823. doi:10.1016/j.celrep.2013.05.014
- Steullet P, Cabungcal JH, Coyle J, Didriksen M, Gill K, Grace AA, Hensch TK, LaMantia AS, Lindemann L, Maynard TM, Meyer U, Morishita H, O'Donnell P, Puhl M, Cuenod M, Do KQ (2017) Oxidative stress-driven parvalbumin interneuron impairment as a common mechanism in models of schizophrenia. *Mol Psychiatry* 22 (7):936-943. doi:10.1038/mp.2017.47
- Sugiyama S, Di Nardo AA, Aizawa S, Matsuo I, Volovitch M, Prochiantz A, Hensch TK (2008) Experience-dependent transfer of Otx2 homeoprotein into the visual cortex activates postnatal plasticity. *Cell* 134 (3):508-520. doi:S0092-8674(08)00839-8 [pii] 10.1016/j.cell.2008.05.054
- Swanson GT, Kamboj SK, Cull-Candy SG (1997) Single-channel properties of recombinant AMPA receptors depend on RNA editing, splice variation, and subunit composition. *J Neurosci* 17 (1):58-69
- Testa D, Prochiantz A, Di Nardo AA (2019) Perineuronal nets in brain physiology and disease. *Semin Cell Dev Biol* 89:125-135. doi:10.1016/j.semcdb.2018.09.011
- Tewari BP, Chaunsali L, Campbell SL, Patel DC, Goode AE, Sontheimer H (2018) Perineuronal nets decrease membrane capacitance of peritumoral fast spiking interneurons in a model of epilepsy. *Nat Commun* 9 (1):4724. doi:10.1038/s41467-018-07113-0
- Tononi G, Cirelli C (2003) Sleep and synaptic homeostasis: a hypothesis. *Brain Res Bull* 62 (2):143-150. doi:10.1016/j.brainresbull.2003.09.004
- Tononi G, Cirelli C (2014) Sleep and the price of plasticity: from synaptic and cellular homeostasis to memory consolidation and integration. *Neuron* 81 (1):12-34. doi:10.1016/j.neuron.2013.12.025
- Uhlhaas PJ, Singer W (2010) Abnormal neural oscillations and synchrony in schizophrenia. *Nat Rev Neurosci* 11 (2):100-113. doi:10.1038/nrn2774
- Van't Spijker HM, Rowlands D, Rossier J, Haenzi B, Fawcett JW, Kwok JCF (2019) Neuronal Pentraxin 2 Binds PNNs and Enhances PNN Formation. *Neural Plast* 2019:6804575. doi:10.1155/2019/6804575
- Vyazovskiy VV, Cirelli C, Pfister-Genskow M, Faraguna U, Tononi G (2008) Molecular and electrophysiological evidence for net synaptic potentiation in wake and depression in sleep. *Nat Neurosci* 11 (2):200-208. doi:10.1038/nn2035
- Wilking M, Ndiaye M, Mukhtar H, Ahmad N (2013) Circadian rhythm connections to oxidative stress: implications for human health. *Antioxid Redox Signal* 19 (2):192-208. doi:10.1089/ars.2012.4889
- Wisor JP (2011) A metabolic-transcriptional network links sleep and cellular energetics in the brain. *Pflugers Arch*. doi:10.1007/s00424-011-1030-6
- Wulff K, Joyce E (2011) Circadian rhythms and cognition in schizophrenia. *Br J Psychiatry* 198 (4):250-252. doi:10.1192/bjp.bp.110.085068

Zhang Z, Sun QQ (2011) Development of NMDA NR2 subunits and their roles in critical period maturation of neocortical GABAergic interneurons. *Dev Neurobiol* 71 (3):221-245.  
doi:10.1002/dneu.20844

## FIGURE LEGENDS

**Figure 1. PNN and PV intensity vary across the diurnal cycle.** (a) Image (428.81  $\mu\text{m}^2$ ) showing WFA+ and PV+ immunolabeling. White arrows are double-labeled cells, yellow arrowheads are single-labeled PV cells (20X). (b) Total WFA intensity in all WFA+ cells was elevated at ZT12 and ZT18 compared with ZT0, and there was a light/dark difference. (c) Similarly, WFA intensity around PV+ cells was elevated at ZT12 and ZT18 compared with ZT0, and there was a light/dark difference. (d) Total PV intensity was decreased in neurons at ZT6 and ZT12 compared with ZT0, and there was a trend for a light/dark difference. (e) PV cell intensity in PV+ cells surrounded by WFA+ was decreased at ZT6 compared with ZT0, and there was a light/dark difference. Data are mean  $\pm$  SEM; N-size: ZT0, N = 10; ZT6, N = 8; ZT12, N = 7; ZT18, N = 8. \* $p < 0.05$  for individual ZTs compared with ZT0 (individual bars) or for light vs. dark comparison (at base of graph); # $p < 0.10$ .

**Figure 2. The oxidative stress marker 8-oxo-dG varies in PV cells with or without PNNs across the diurnal cycle.** (a) Image (428.81  $\mu\text{m}^2$ ) showing 8-oxo-dG+, WFA+, and PV+ immunolabeling. White arrows are triple-labeled cells; yellow arrow is single-labeled 8-oxo-dG cell (20X). (b) Total 8-oxo-dG was decreased at all ZTs compared with ZT0, and there was a light/dark difference. (c) Triple-labeled 8-oxo-dG+/WFA+/PV+ cells demonstrated a decrease at all ZTs compared with ZT0, and there was a light/dark difference. (d) Double-labeled 8-oxo-dG+/WFA+ cells demonstrated a decrease at all ZTs compared with ZT0, and there was a light/dark difference. (e) Double-labeled 8-oxo-dG+/PV+ cells demonstrated a decrease at all ZTs compared with ZT0, and there was a light/dark difference. (f) 8-oxo-dG+/PV+ cells showed higher oxidative stress levels than 8-oxo-dG+/WFA+ cells at ZT6 and ZT12. Each group of double-labeled cells was normalized to its own ZT0 value; dotted line is normalized ZT0 value. Data are mean  $\pm$  SEM; N-size: ZT0, N = 4; ZT6, N = 4; ZT12, N = 3; ZT18, N = 4. For B-E, \* $p <$

0.05 compared with ZT0 for individual ZTs compared with ZT0 (individual bars) or for light vs. dark comparison (at base of graph); for (F), \* $p < 0.05$  compared with 8-oxo-dG/WFA+ cells within the same ZT.

**Figure 3. The number of glutamatergic puncta apposing PV neurons with PNNs increases at ZT18, and PV cell volume increases at ZT18**

(a) An immunolabeled PV neuron (red) is surrounded by a WFA-labeled PNN (blue) in a representative confocal micrograph from the mPFC. The PV neuron is receiving appositions from both vGLUT1-labeled glutamatergic puncta (magenta) and GAD65/67-labeled GABAergic puncta (green). (b) The Imaris *Surfaces* segmentation tool was used to render the PV neuron (gray) and WFA-labeled PNN (blue). The Imaris *Spots* segmentation tool was used to segment GAD65/67 (green arrows) and vGLUT1-labeled (magenta arrows) puncta that met size and location criteria. Scale bar = 5  $\mu$ m. **In WFA+/PV+ cells:** (c) Number of inhibitory puncta (GAD65/67) were similar at ZT6 and ZT18. (d) Number of excitatory puncta (vGLUT1) apposing PV neurons was higher at ZT18 compared with ZT6. (e) The ratio of GAD65/67:vGLUT1 puncta trended toward a decrease at ZT18 compared with ZT6. (f) The volumes of the three-dimensional surfaces rendered with Imaris software through the middle of the PV neurons were larger at ZT18 compared with those at ZT6. **In WFA-/PV+ cells:** (g) Number of inhibitory puncta (GAD65/67) was similar in the ZT6 and ZT18 groups. (h) Number of excitatory puncta (vGLUT1) was similar at ZT6 and ZT18. (i) The ratio of GAD65/67:vGLUT1 puncta was similar at ZT6 and ZT18. (j) The volumes of the three-dimensional surfaces rendered with Imaris software were similar at ZT6 and ZT18. Data are mean  $\pm$  SEM; N = 4/group. \* $p < 0.05$  compared with ZT6; # $p < 0.10$  compared with ZT6.

**Figure 4. The AMPA:NMDA ratio increases at ZT18.**

(a) Representative traces of the AMPA (black) and NMDA (green) components at ZT6 and ZT18. Scale bar represents 10 pA, 10ms. (b) AMPA:NMDA ratio of mEPSCs evoked from PNN-surrounded fast-spiking cells in the



prelimbic mPFC increases during the dark phase at ZT18. (c) Average time constants of decay of the NMDA component of mEPSCs evoked from PNN surrounded PV FSIs in the prelimbic mPFC. Data are mean  $\pm$  SEM; Number of rats: ZT6 N = 7; ZT18 N = 8. \*p < 0.05; #p < 0.10 compared with ZT6.

**Figure 5. OTX2 staining in PV+ cells and WFA+/PV+ cells trend toward increase at ZT18.**

(a) Image (428.81  $\mu\text{m}^2$ ) showing OTX2+, WFA+, and PV+ immunolabeling. White arrows are triple-labeled cells, yellow arrowhead is double-labeled OTX2+/PV+ cell, and white arrowhead is double-labeled OTX2/WFA+ cell (20X). (b) Total number of OTX2+ cells was similar at ZT6 and ZT18. (c) Number of OTX2+/WFA+ cells was similar at ZT6 and ZT18. (d) Number of OTX2+/PV+ cells showed a strong trend toward increase at ZT18 compared with ZT6. (e) Number of OTX2+/WFA+/PV+ cells showed a trend toward increase at ZT18 compared with ZT6. Data are mean  $\pm$  SEM; N = 6-7/group. #p < 0.10 compared with ZT6.

Figure 1

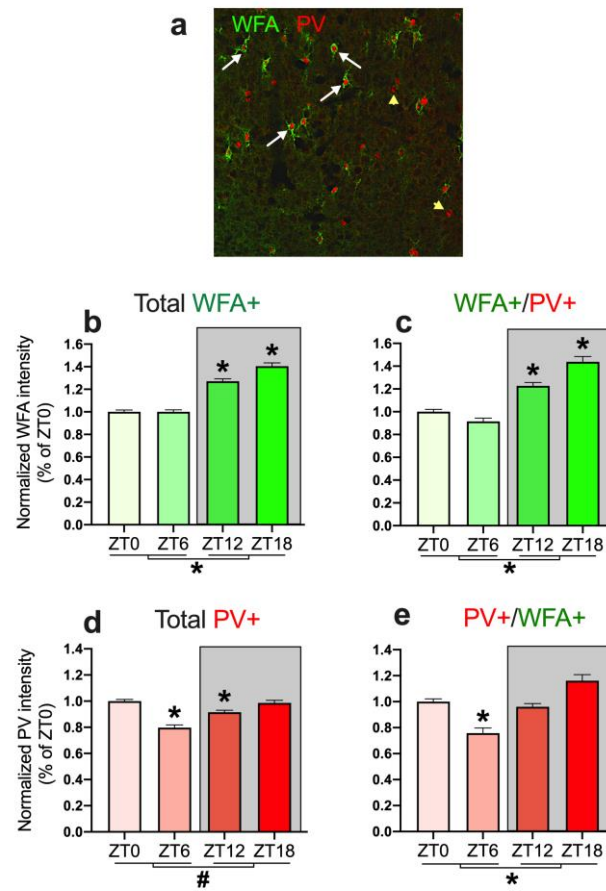


**Figure 2**

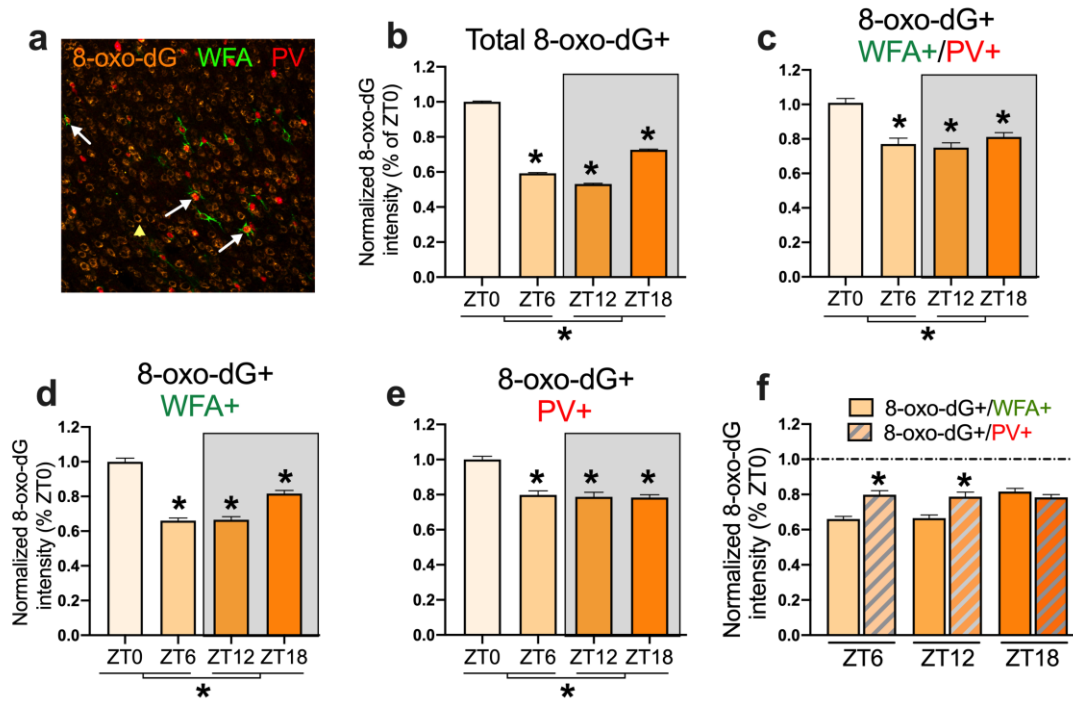
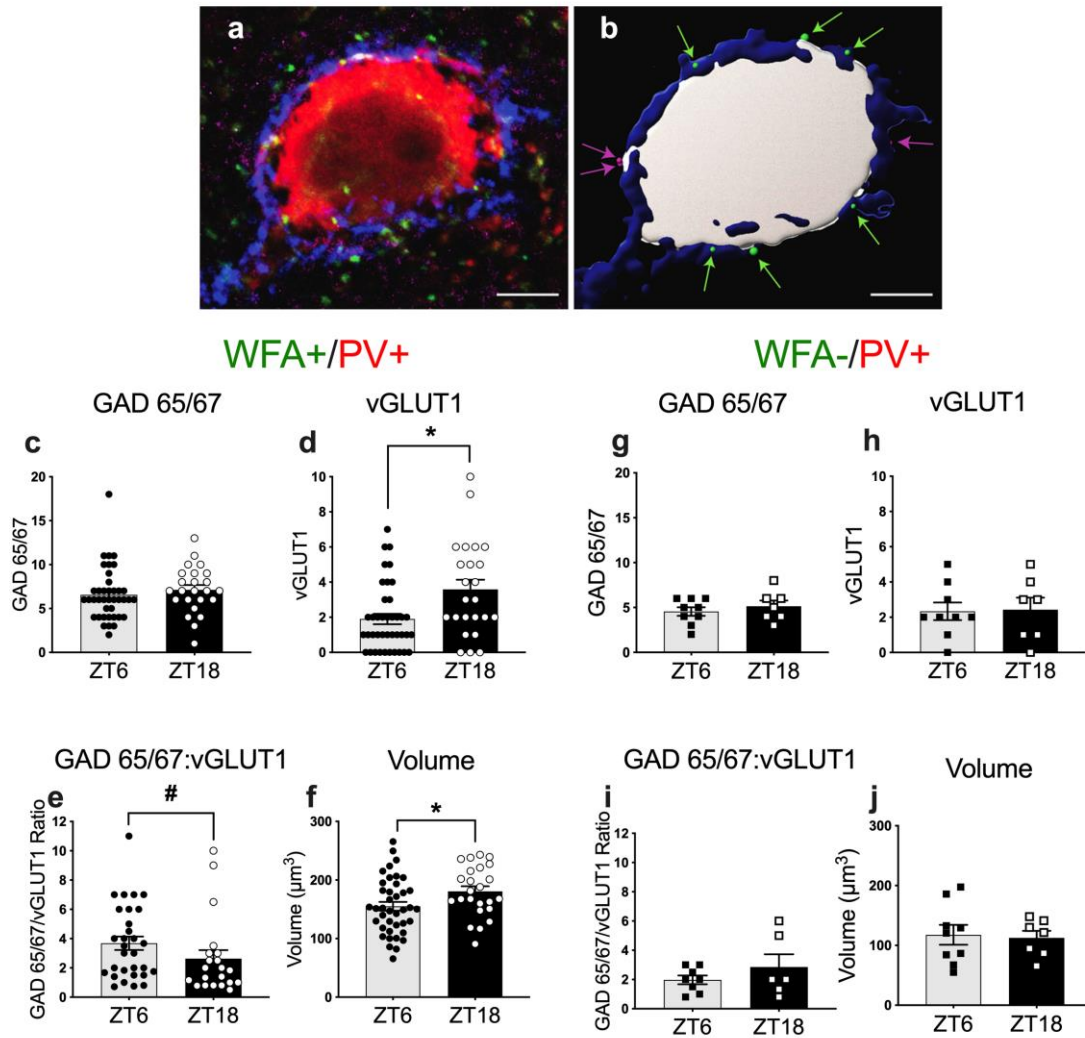
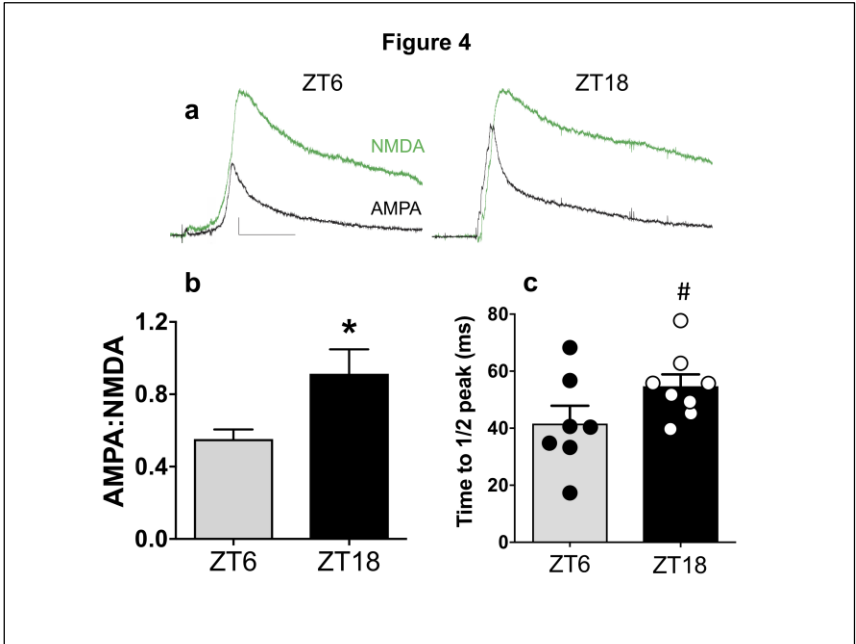
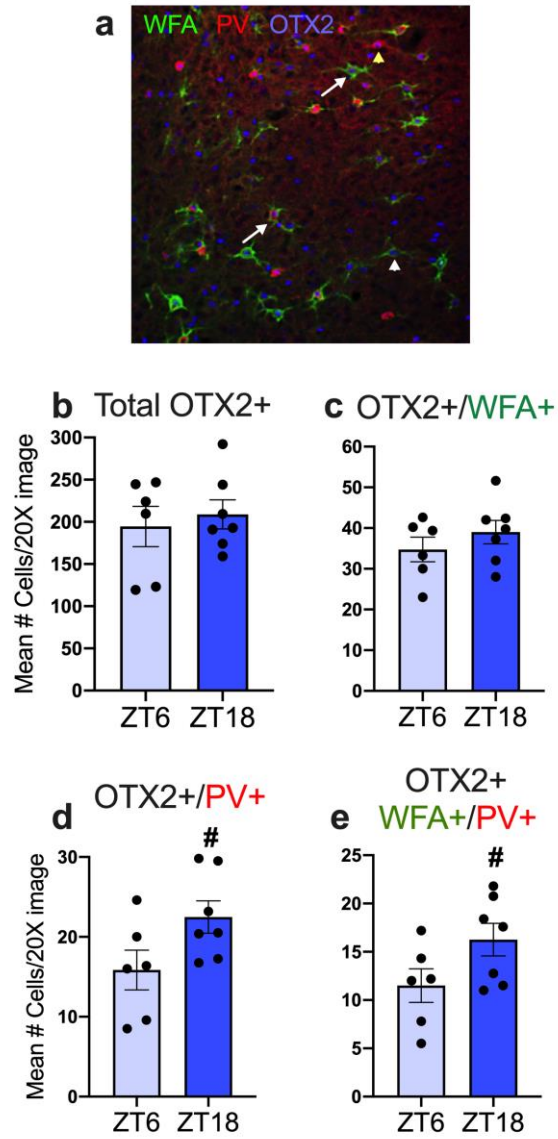


Figure 3





**Figure 5**



**Table 1: Number and percent of WFA/PV cells**

<b>Stain</b>	<b>ZT0</b>	<b>ZT6</b>	<b>ZT12</b>	<b>ZT18</b>
Total WFA+	24.4 ± 1.5	24.2 ± 1.7	25.6 ± 2.8	22.8 ± 2.35
#Total PV+	30.0 ± 2.7	18.2 ± 1.4	27.6 ± 3.3	23.7 ± 5.0
WFA+/PV-	10.4 ± 1.3	16.2 ± 2.0	12.5 ± 2.9	12.2 ± 0.7
WFA-/PV+	16.0 ± 1.7	10.2 ± 1.3	14.6 ± 1.4	13.1 ± 2.9
*WFA+/PV+	13.9 ± 1.1	8.0 ± 0.7	13.0 ± 2.1	10.6 ± 2.2
<b>% Co-localization</b>				
% WFA cells with PV	57.8 ± 4.2	<b>34.7 ± 4.2*</b>	52.9 ± 8.4	43.4 ± 5.2
% PV cells with WFA	47.4 ± 2.2	45.2 ± 4.0	45.5 ± 3.4	45.9 ± 2.3

Significant differences are in bold font. \*P < 0.05 vs. ZT0; #p < 0.10 for one-way ANOVA

Table 2: Number and percent of 8-oxo-dG cells

Stain	ZT0	ZT6	ZT12	ZT18
Total 8-oxo-dG+	333.9 ± 14.7	295.5 ± 50.8	330.7 ± 33.0	339.1 ± 30.5
8-oxo-dG+/WFA+	24.5 ± 1.4	23.0 ± 1.4	28.6 ± 2.5	24.6 ± 3.0
8-oxo-dG+/WFA-	310.7 ± 14.6	272.5 ± 48.7	298.4 ± 35.5	314.5 ± 28.0
8-oxo-dG+/PV+	23.8 ± 2.2	<b>11.8 ± 1.5*</b>	<b>13.6 ± 3.4*</b>	22.4 ± 2.1
8-oxo-dG+/PV-	311.3 ± 13.3	283.7 ± 51.6	313.3 ± 36.4	316.7 ± 28.8
8-oxo-dG+/WFA+/PV+	15.4 ± 0.7	<b>6.3 ± 0.5*</b>	10.3 ± 3.7	14.5 ± 2.2
<b>% Co-localization</b>				
<b>% of 8-oxo-dG+ cells</b>				
with WFA+	7.3 ± 0.5	8.1 ± 0.7	9.1 ± 1.5	7.2 ± 0.4
with PV+	7.0 ± 0.5	4.5 ± 1.1	4.6 ± 1.4	6.6 ± 0.4
with WFA+/PV+	4.5 ± 0.1	2.3 ± 0.4	3.5 ± 1.4	4.2 ± 0.5
<b>% of WFA+ cells</b>				
with 8-oxo-dG+	<b>87.0 ± 1.3<sup>1</sup></b>	<b>85.5 ± 1.9<sup>1</sup></b>	<b>91.6 ± 0.4<sup>2</sup></b>	<b>90.0 ± 1.6<sup>2</sup></b>
<b>% of PV+ cells</b>				
with 8-oxo-dG+	59.3 ± 4.9	56.9 ± 1.1	55.5 ± 4.3	58.2 ± 4.1
<b>% of WFA+/PV+ cells</b>				
with 8-oxo-dG	94.7 ± 1.3	93.1 ± 1.6	93.7 ± 2.5	96.2 ± 0.1

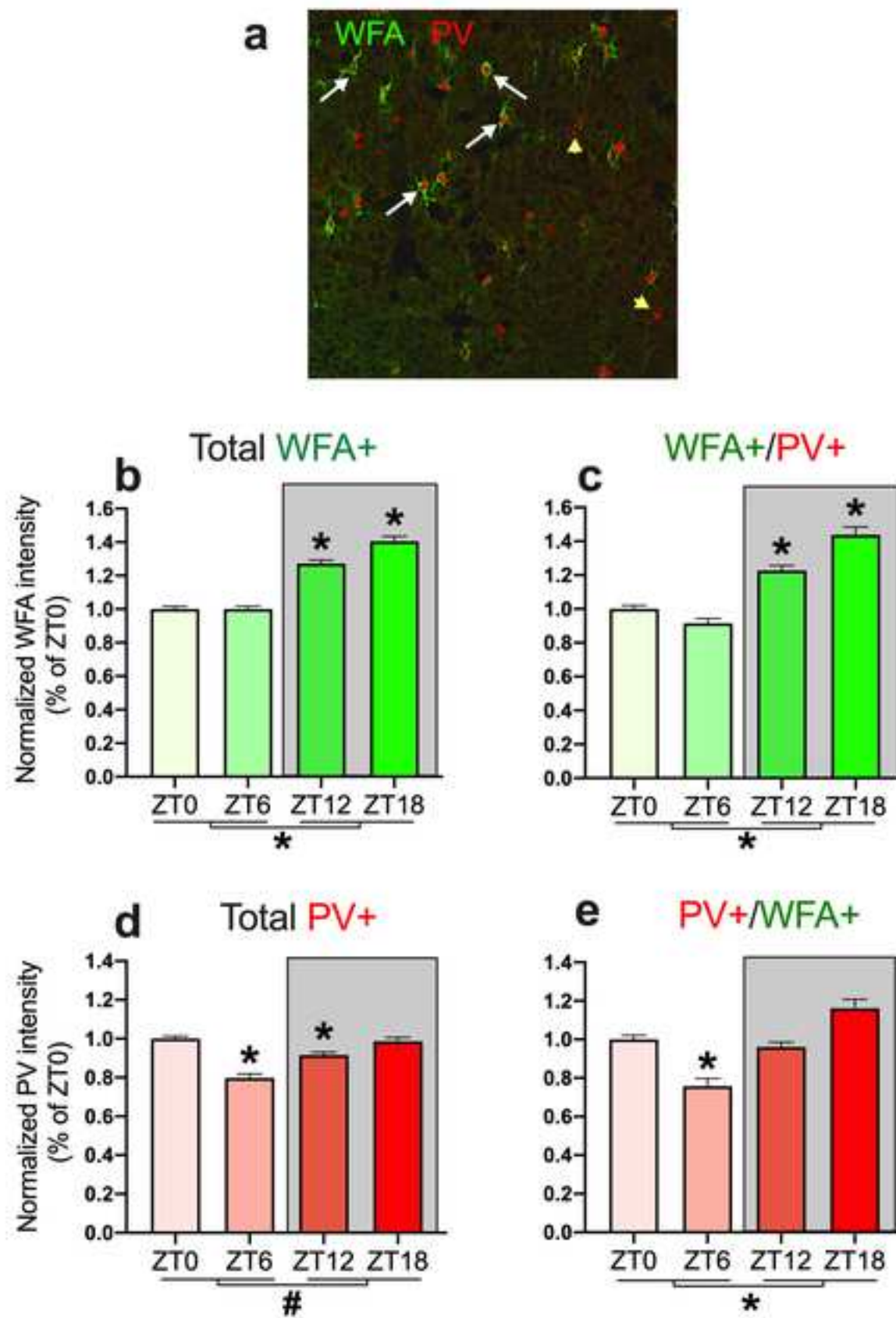
Significant differences are in bold font. Numbers <sup>1,2</sup> denote difference between light (ZT0 + ZT6) and dark (ZT12 + ZT18). \*P < 0.05 vs. ZT0.



**Table 3: Number and percent of Otx2 cells**

<b>Stain</b>	<b>ZT6</b>	<b>ZT18</b>
Total Otx2+	194.6 ± 23.9	208.8 ± 17.2
Otx2+/WFA+	34.7 ± 3.0	39.0 ± 2.9
Otx2+/WFA-	159.8 ± 21.5	169.8 ± 14.9
Otx2+/PV+	15.9 ± 2.5	<b>22.5 ± 2.0<sup>#</sup></b>
Otx2+/PV-	178.7 ± 25.9	186.4 ± 16.3
Otx2+/WFA+/PV+	11.5 ± 1.7	<b>16.3 ± 1.7<sup>#</sup></b>
<b>% Co-localization</b>		
<b>% of Otx2+ cells</b>		
with WFA+	18.6 ± 1.4	18.8 ± 0.8
with PV+	9.8 ± 2.8	11.0 ± 0.9
with WFA+/PV+	7.0 ± 2.0	7.8 ± 0.7
<b>% of WFA+ cells</b>		
with Otx2	71.5 ± 1.3	67.3 ± 2.2
<b>% of PV+ cells</b>		
with Otx2	72.4 ± 3.4	70.2 ± 4.2
<b>% of WFA+/PV+ cells</b>		
with Otx2	92.5 ± 1.5	93.9 ± 1.9

<sup>#</sup>p < 0.10 vs. ZT6.

**Figure 1**

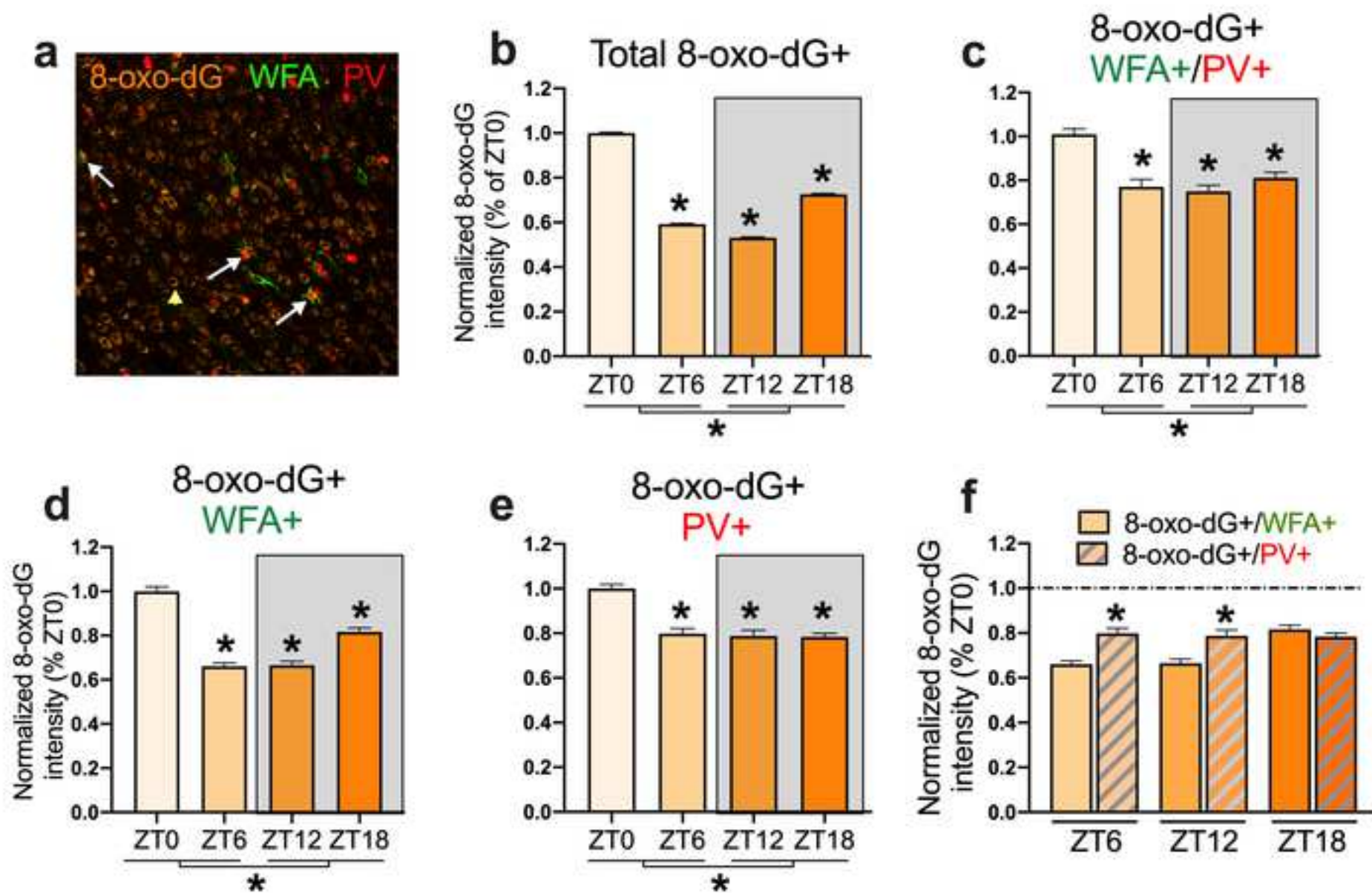
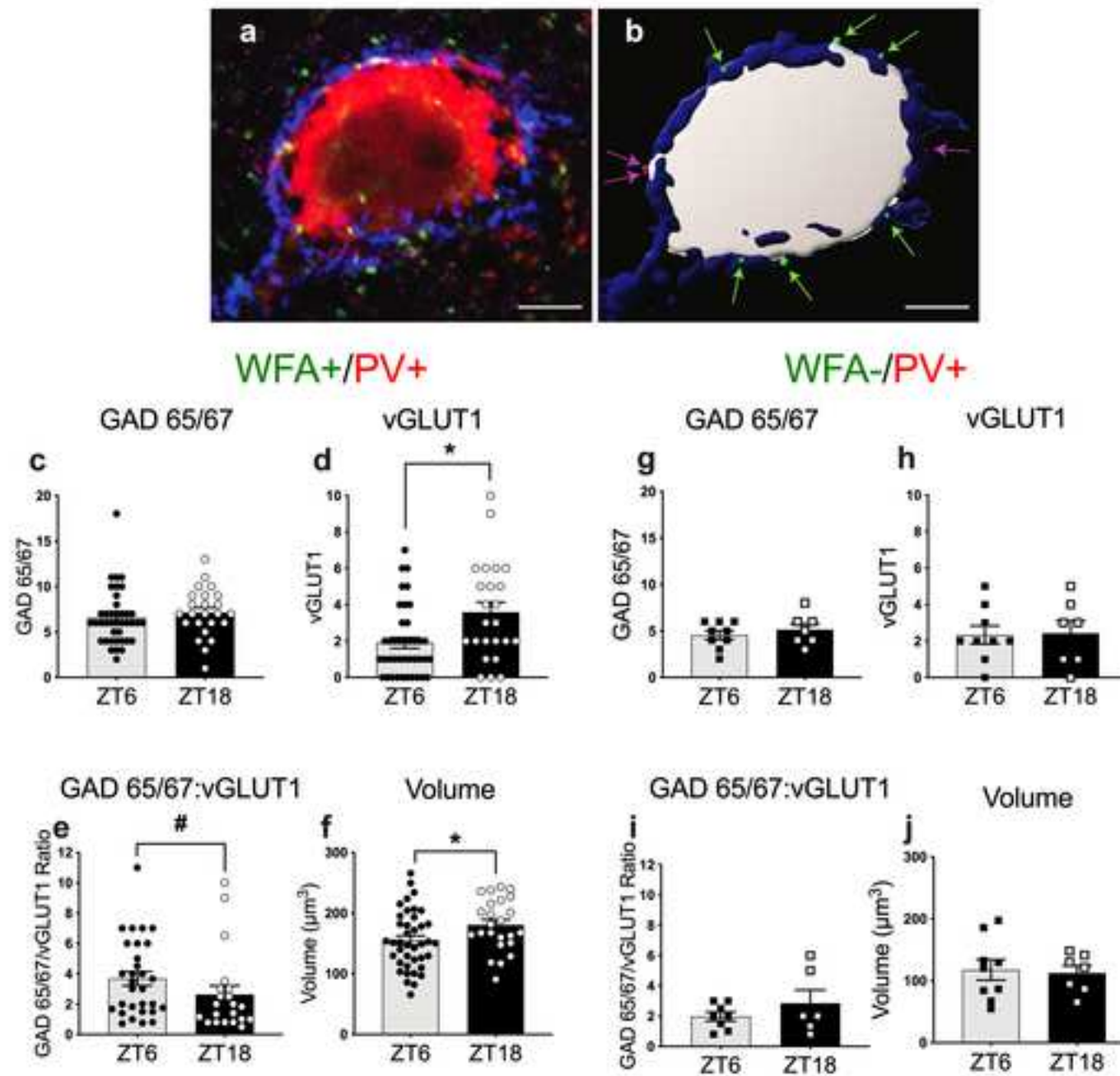
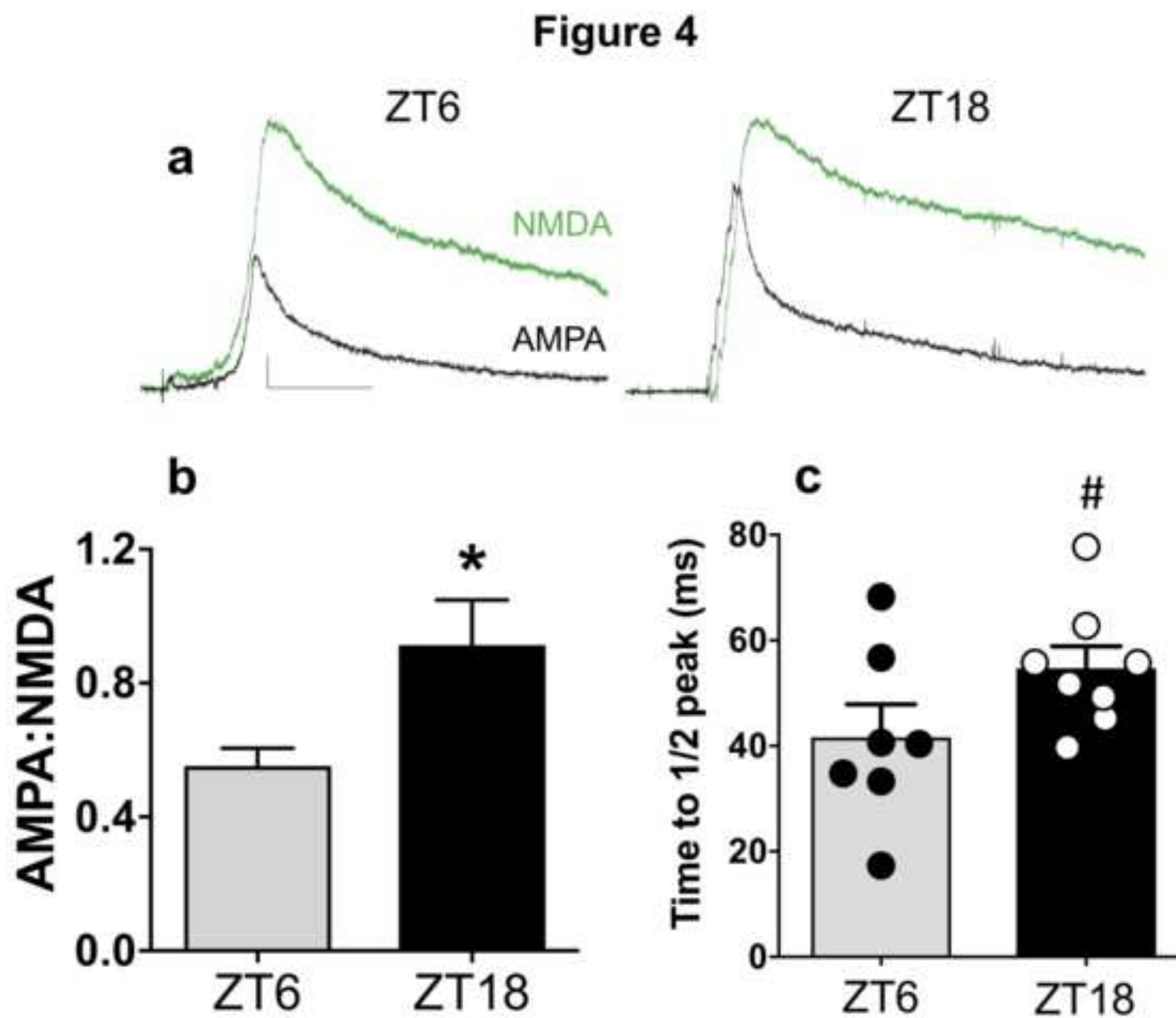
**Figure 2**

Figure 3







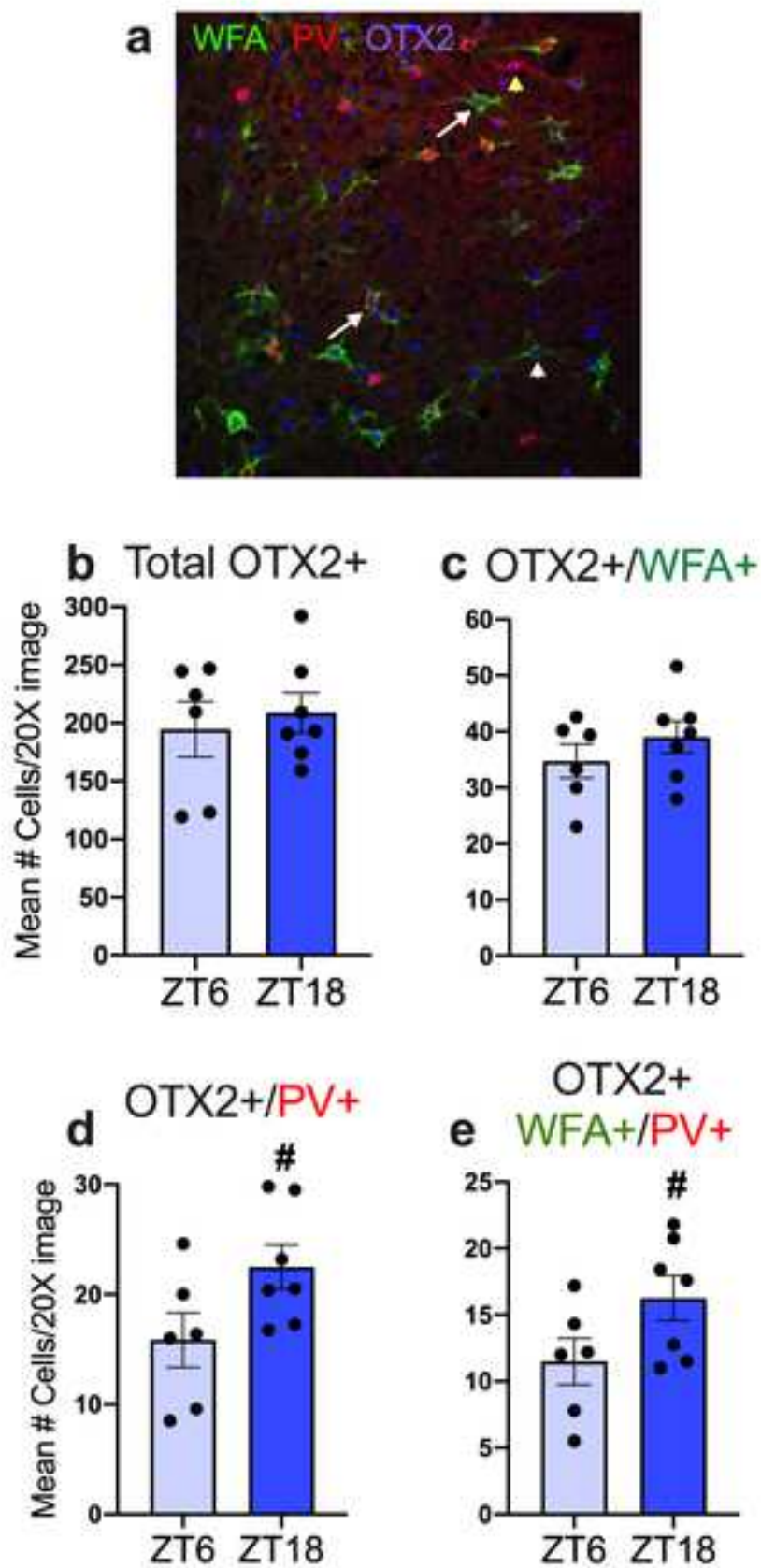
**Figure 5**

Table 1: Number and percent of WFA/PV cells

Stain	ZT0	ZT6	ZT12	ZT18
Total WFA+	24.4 ± 1.5	24.2 ± 1.7	25.6 ± 2.8	22.8 ± 2.35
#Total PV+	30.0 ± 2.7	18.2 ± 1.4	27.6 ± 3.3	23.7 ± 5.0
WFA+/PV-	10.4 ± 1.3	16.2 ± 2.0	12.5 ± 2.9	12.2 ± 0.7
WFA-/PV+	16.0 ± 1.7	10.2 ± 1.3	14.6 ± 1.4	13.1 ± 2.9
#WFA+/PV+	13.9 ± 1.1	8.0 ± 0.7	13.0 ± 2.1	10.6 ± 2.2
% Co-localization				
% WFA cells with PV	57.8 ± 4.2	<b>34.7 ± 4.2*</b>	52.9 ± 8.4	43.4 ± 5.2
% PV cells with WFA	47.4 ± 2.2	45.2 ± 4.0	45.5 ± 3.4	45.9 ± 2.3

Significant differences are in bold font. \*P < 0.05 vs. ZT0; #p < 0.10 for one-way ANOVA

**Table 2: Number and percent of 8-oxo-dG cells**

Stain	ZT0	ZT6	ZT12	ZT18
Total 8-oxo-dG+	333.9 ± 14.7	295.5 ± 50.8	330.7 ± 33.0	339.1 ± 30.5
8-oxo-dG+/WFA+	24.5 ± 1.4	23.0 ± 1.4	28.6 ± 2.5	24.6 ± 3.0
8-oxo-dG+/WFA-	310.7 ± 14.6	272.5 ± 48.7	298.4 ± 35.5	314.5 ± 28.0
8-oxo-dG+/PV+	23.8 ± 2.2	<b>11.8 ± 1.5*</b>	<b>13.6 ± 3.4*</b>	22.4 ± 2.1
8-oxo-dG+/PV-	311.3 ± 13.3	283.7 ± 51.6	313.3 ± 36.4	316.7 ± 28.8
8-oxo-dG+/WFA+/PV+	15.4 ± 0.7	<b>6.3 ± 0.5*</b>	10.3 ± 3.7	14.5 ± 2.2
<b>% Co-localization</b>				
<b>% of 8-oxo-dG+ cells</b>				
with WFA+	7.3 ± 0.5	8.1 ± 0.7	9.1 ± 1.5	7.2 ± 0.4
with PV+	7.0 ± 0.5	4.5 ± 1.1	4.6 ± 1.4	6.6 ± 0.4
with WFA+/PV+	4.5 ± 0.1	2.3 ± 0.4	3.5 ± 1.4	4.2 ± 0.5
<b>% of WFA+ cells</b>				
with 8-oxo-dG+	<b>87.0 ± 1.3<sup>1</sup></b>	<b>85.5 ± 1.9<sup>1</sup></b>	<b>91.6 ± 0.4<sup>2</sup></b>	<b>90.0 ± 1.6<sup>2</sup></b>
<b>% of PV+ cells</b>				
with 8-oxo-dG+	59.3 ± 4.9	56.9 ± 1.1	55.5 ± 4.3	58.2 ± 4.1
<b>% of WFA+/PV+ cells</b>				
with 8-oxo-dG	94.7 ± 1.3	93.1 ± 1.6	93.7 ± 2.5	96.2 ± 0.1

Significant differences are in bold font. Numbers <sup>1,2</sup> denote difference between light (ZT0 + ZT6) and dark (ZT12 + ZT18). \*P < 0.05 from ZT0.



**Table 3: Number and percent of Otx2 cells**

Stain	ZT6	ZT18
Total Otx2+	194.6 ± 23.9	208.8 ± 17.2
Otx2+/WFA+	34.7 ± 3.0	39.0 ± 2.9
Otx2+/WFA-	159.8 ± 21.5	169.8 ± 14.9
Otx2+/PV+	15.9 ± 2.5	<b>22.5 ± 2.0<sup>#</sup></b>
Otx2+/PV-	178.7 ± 25.9	186.4 ± 16.3
Otx2+/WFA+/PV+	11.5 ± 1.7	<b>16.3 ± 1.7<sup>#</sup></b>
<b>% Co-localization</b>		
<b>% of Otx2+ cells</b>		
with WFA+	18.6 ± 1.4	18.8 ± 0.8
with PV+	9.8 ± 2.8	11.0 ± 0.9
with WFA+/PV+	7.0 ± 2.0	7.8 ± 0.7
<b>% of WFA+ cells</b>		
with Otx2	71.5 ± 1.3	67.3 ± 2.2
<b>% of PV+ cells</b>		
with Otx2	72.4 ± 3.4	70.2 ± 4.2
<b>% of WFA+/PV+ cells</b>		
with Otx2	92.5 ± 1.5	93.9 ± 1.9

<sup>#</sup>p < 0.10.